





19 Concentrated agricultural activities and animal feeding operations in the northeastern  
20 plains of Colorado represent an important source of atmospheric ammonia ( $\text{NH}_3$ ) that  
21 contributes to regional fine particle formation and to nitrogen deposition to sensitive  
22 ecosystems in Rocky Mountain National Park (RMNP) located ~80 km to the west. In  
23 order to better understand temporal and spatial differences in  $\text{NH}_3$  concentrations in this  
24 source region, weekly concentrations of  $\text{NH}_3$  were measured at 14 locations during the  
25 summers of 2010 to 2015 using Radiello passive  $\text{NH}_3$  samplers. Weekly (biweekly in 2015)  
26 average  $\text{NH}_3$  concentrations ranged from  $2.66 \mu\text{g}/\text{m}^3$  to  $42.7 \mu\text{g}/\text{m}^3$  with the highest  
27 concentrations near large concentrated animal feeding operations (CAFOs). The annual  
28 summertime mean  $\text{NH}_3$  concentrations were stable in this region from 2010 to 2015,  
29 providing a baseline against which concentration changes associated with future changes  
30 in regional  $\text{NH}_3$  emissions can be assessed. Vertical profiles of  $\text{NH}_3$  were also measured  
31 on the 300 m Boulder Atmospheric Observatory (BAO) tower throughout 2012. The  
32 highest  $\text{NH}_3$  concentration along the vertical profile was always observed at the 10 m  
33 height (annual average concentration of  $4.63 \mu\text{g}/\text{m}^3$ ), decreasing toward the surface ( $4.35$   
34  $\mu\text{g}/\text{m}^3$ ) and toward higher altitudes ( $1.93 \mu\text{g}/\text{m}^3$ ). Seasonal changes in the steepness of the  
35 vertical concentration gradient were observed, with the sharpest gradients in cooler seasons  
36 when thermal inversions restricted vertical mixing of surface-based emissions. The  $\text{NH}_3$   
37 spatial distributions measured using the passive samplers are compared with  $\text{NH}_3$  columns  
38 retrieved by the Infrared Atmospheric Sounding Interferometer (IASI) satellite and  
39 concentrations simulated by the Comprehensive Air quality Model with extensions  
40 (CAMx), providing insight into the regional performance of each. The satellite comparison  
41 adds to a growing body of evidence that IASI column retrievals of  $\text{NH}_3$  provide very useful



42 insight into regional variability in atmospheric  $\text{NH}_3$ , in this case even in a region with  
43 strong local sources and sharp spatial gradients. The CAMx comparison indicates that the  
44 model does a reasonable job simulating  $\text{NH}_3$  concentrations near sources but tends to  
45 underpredict concentrations at locations farther downwind. Excess  $\text{NH}_3$  deposition by the  
46 model is hypothesized as a possible explanation for this trend.

47

## 48 **1. Introduction**

49

50 As the most abundant basic gas in the atmosphere, ammonia ( $\text{NH}_3$ ) can neutralize ambient  
51 acidic species, such as sulfuric acid ( $\text{H}_2\text{SO}_4$ ) and nitric acid ( $\text{HNO}_3$ ), to form ammonium  
52 salts, which are the dominant inorganic compounds in ambient  $\text{PM}_{2.5}$  (particulate matter  
53 with aerodynamic diameter less than  $2.5 \mu\text{m}$ ).  $\text{PM}_{2.5}$  has been linked to adverse effects on  
54 human health and regional visibility reduction and also impacts climate via direct and  
55 indirect changes in radiative forcing (Davidson et al., 2005;Langridge et al., 2012;Park et  
56 al., 2006;Parry et al., 2007;Schwartz and Neas, 2000;Lelieveld et al., 2015). The  
57 atmospheric lifetime of  $\text{NH}_3$  is short, on the order of hours to days, due to rapid dry  
58 deposition and particle-forming chemical reactions; ammonium ( $\text{NH}_4^+$ ) salts which are  
59 primarily found in submicron aerosol particles have longer atmospheric lifetimes (on the  
60 order of several days) and can be transported to remote areas away from ammonia sources  
61 (Aneja et al., 2001;Fowler et al., 1998;Ianniello et al., 2011). Dry and wet deposition of  
62  $\text{NH}_3$  and  $\text{NH}_4^+$  also play an important role in the adverse effects of increased nitrogen  
63 deposition to sensitive ecosystems (Asman et al., 1998;Beem et al., 2010;Benedict et al.,  
64 2013a;Horii et al., 2006;Paulot et al., 2013).



65

66 It is widely believed that agriculture represents the largest source of  $\text{NH}_3$  globally, but at  
67 smaller spatial scales the influence of ag will vary greatly. Sutton et al. (2013) estimate that  
68 57% of global atmospheric  $\text{NH}_3$  is emitted from livestock and crops, while the U.S.  
69 Environmental Protection Agency (EPA) attributes over 85% of  $\text{NH}_3$  emissions in the U.S.  
70 to the agricultural sector (EPA, 1998). Hertel et al. (2006) also found that deposition of  
71 atmospheric  $\text{NH}_3$  near an intensive agricultural area would dominate the overall load of  
72 reactive nitrogen (N) from the atmosphere. Agricultural  $\text{NH}_3$  emissions have become one  
73 of the most significant air pollution problems in recent years and have attracted growing  
74 concern from environmental scientists and government regulators (Aneja et al., 2006; Pan  
75 et al., 2012; Bauer et al., 2016).

76

77 The northeastern plains of Colorado include the Denver-Fort Collins urban corridor along  
78 the Front Range\* and a large agricultural region reaching eastward toward the border with  
79 Nebraska. This area has been recognized as an important  $\text{NH}_3$  emission source region, and  
80 the largest reduced nitrogen source near Rocky Mountain National Park (RMNP) (Benedict  
81 et al., 2013b; Ellis et al., 2013). In 2002,  $\text{NH}_3$  emissions from the Front Range were  
82 estimated to be 10288 tons/year from livestock and 5183 tons/year from fertilizer  
83 application, which accounted for 30% and 27% of Colorado's  $\text{NH}_3$  emissions, respectively  
84 (according to RMNP Initiative – Nitrogen Deposition Reduction Contingency Plan, 2010).  
85 The Rocky Mountain Atmospheric Nitrogen and Sulfur (RoMANS) studies, conducted in

---

\* The Front Range is defined here as the following 10 counties in Colorado: Adams, Arapahoe, Boulder, Broomfield, Denver, Douglas, El Paso, Jefferson, Larimer and Weld.



86 2006 and 2009, showed that both  $\text{NH}_3$  and  $\text{NH}_4^+$  contributed approximately 50% of the  
87 total reactive nitrogen deposition (both wet and dry) in RMNP, with the balance coming  
88 from dry and wet deposition of nitrate and organic nitrogen. The highest concentrations of  
89 ammonium particles were associated with upslope transport from the east side of RMNP,  
90 indicating major sources of  $\text{NH}_3$  to RMNP are located in the northeastern plains of  
91 Colorado (Benedict et al., 2013b; Beem et al., 2010; Eilerman et al., 2016). In 2010 an effort  
92 was initiated to map the  $\text{NH}_3$  concentrations in Northern Colorado and significant  $\text{NH}_3$   
93 spatial differences were found, with averages ranging from  $3.43 \mu\text{g}/\text{m}^3$  at rural grasslands  
94 to  $10.7 \mu\text{g}/\text{m}^3$  at suburban-urban sites and  $31.5 \mu\text{g}/\text{m}^3$  near an area of concentrated animal  
95 feeding operations (CAFOs) (Day et al., 2012).

96

97 Due to the short atmospheric lifetime and high dry deposition velocity of  $\text{NH}_3$ , there are  
98 many factors, such as the height of the boundary layer, surface properties, location of  
99 sources, local advection and the vertical mixing rate, that influence spatial (horizontal and  
100 vertical) distributions of  $\text{NH}_3$  concentrations. This complex dependence of  $\text{NH}_3$   
101 concentrations on atmospheric conditions and deposition variables results in great  
102 uncertainties of  $\text{NH}_3$  concentrations in global and regional atmospheric chemistry models  
103 (Sutton et al., 2008; Zhu et al., 2013). The primary goal of this study is to investigate the  
104 spatial and temporal variability of  $\text{NH}_3$  concentrations in the northeastern plains of  
105 Colorado. This effort builds upon the earlier efforts of Benedict et al. (2013b), Day et al.  
106 (2012), and Battye et al. (2016) to look at patterns of spatial variability across several years  
107 with different meteorology and source strength (e.g., years with and without active fire  
108 seasons) and to identify any multi-year trends in regional ammonia concentrations. Year-



109 round measurements of the vertical profile of  $\text{NH}_3$  measured using a 300 m tower near Erie,  
110 Colorado will also provide new insight into the vertical profile of ammonia concentrations  
111 in the lower atmosphere and its change with season. The *in situ* surface and tower  
112 measurements will also be used to examine ammonia remote sensing measurements from  
113 the Infrared Atmospheric Sounding Interferometer (IASI) satellite (Whitburn et al.,  
114 2016; Van Damme et al., 2015) and predictions from the Comprehensive Air quality Model  
115 with extensions (CAMx) to provide insight into the regional performance of each. Overall  
116 our results are useful for determining important sources contributing to regional nitrogen  
117 deposition, validating emission inventories and concentration predictions for atmospheric  
118 chemistry models and setting a baseline against which concentration changes resulting  
119 from future emission changes can be assessed.

120

## 121 **2. Methodology**

### 122 **2.1 Site descriptions**

123

124 The northeastern plains of Colorado are an intensive agricultural area with many CAFOs,  
125 including beef cattle feedlots and dairy operations. The densely populated Front Range  
126 urban corridor is located just west of this area with the Rocky Mountains immediately west  
127 of the urban corridor. In order to gain information about spatial variability of northeast  
128 Colorado ammonia concentrations, fourteen monitoring sites were selected in the region  
129 according to land use categories and distance from known, major  $\text{NH}_3$  sources (Table 1).  
130 Five suburban monitoring sites located in the western part of northeast Colorado are  
131 representative of areas with little local agricultural influence, especially from animal



132 feeding operations: Louisville (LE), western Fort Collins (FC\_W), Loveland (LD),  
133 Loveland Golf Course (LGC) and the Boulder Atmospheric Observatory (BAO) tower.  
134 Three rural sites (Nunn, NN; Briggsdale, BE; and Ranch, RH), close to the northern  
135 boundary of Colorado with Wyoming, are grassland sites with minimal local agricultural  
136 influence. Three suburban sites (eastern Fort Collins, FC\_E; Severance, SE; and Greeley,  
137 GY) as well as three rural sites (Ault, AT; Kersey, KY; and Brush, BH) represent areas  
138 close to and likely significantly influenced by agricultural activities, including animal  
139 feeding operations. For example, the KY site is located approximately 0.4 km from a large  
140 beef cattle feedlot (about 100,000 cattle capacity).

141

142 The BAO tower is a 300 m meteorological tower situated in the southern part of the  
143 sampling area (40.050N, 105.004W). It has been owned and operated by the National  
144 Oceanic and Atmospheric Administration (NOAA) for more than 25 years  
145 (<http://www.esrl.noaa.gov/psd/technology/bao/>). The tower is surrounded by natural grass  
146 and wheat fields, and is approximately 400 m west of Interstate 25 and 30 km north of  
147 downtown Denver.

148

## 149 **2.2 Sample collection and validation**

150

151 In order to obtain spatial and vertical distributions of NH<sub>3</sub> concentrations, two sampling  
152 campaigns were carried out in the northeastern plains of Colorado using Radiello passive  
153 NH<sub>3</sub> samplers and URG (University Research Glassware, Inc.) denuder/filter-pack systems.  
154 The Radiello passive NH<sub>3</sub> sampler consists of a cartridge adsorbent (part number:



155 RAD168), a blue microporous cylindrical diffusive body (part number: RAD1201) and a  
156 vertical adapter (part number: RAD 122). All Radiello sampler components were obtained  
157 from Sigma Aldrich (<http://www.sigmaaldrich.com>). Measurements of the spatial NH<sub>3</sub>  
158 distribution were conducted each summer from 2010 to 2015. During the first summer  
159 (2010), measurements were made at nine sites; in 2011, the Ranch (RH) site was removed  
160 and the LE and NN sites were added; in 2012, the LE site was removed; two sites, FC\_E  
161 and SE, were added in 2013. The two site (RH and LE) removals in 2013 and FC\_E  
162 removal in 2015 were both due to property access issues. In a second campaign,  
163 measurements of vertical NH<sub>3</sub> concentration profiles were conducted at the BAO tower  
164 from December 2011 to January 2013.

165

### 166 **2.2.1 Passive sampler**

167

168 Passive ammonia samplers have been used in several studies because of their reliability,  
169 low labor intensity, simplicity and lack of power requirement (Cisneros et al., 2010; Day et  
170 al., 2012; Meng et al., 2011; Reche et al., 2012; Puchalski et al., 2011). During sample  
171 collection, the sampler was protected from precipitation and direct sunlight by an inverted  
172 plastic bucket. Ambient NH<sub>3</sub> diffuses through a microporous diffusive body surface and is  
173 captured as ammonium ion by a cartridge impregnated with phosphoric acid (H<sub>3</sub>PO<sub>4</sub>). A  
174 weekly sampling campaign period was implemented in each summer during the study: May  
175 20<sup>th</sup> to September 2<sup>nd</sup> 2010, June 2<sup>nd</sup> to August 31<sup>st</sup> 2011, June 21<sup>st</sup> to August 29<sup>th</sup> 2012,  
176 May 30<sup>th</sup> to August 29<sup>th</sup> 2013 and May 29<sup>th</sup> to August 28<sup>th</sup> 2014. Bi-weekly samples were  
177 collected from May 26<sup>th</sup> to September 1<sup>st</sup> 2015. At the BAO tower, NH<sub>3</sub> was sampled at



178 nine heights: 1 m, 10 m, 22 m, 50 m, 100 m, 150 m, 200 m, 250 m, and 300 m. Vertical  
179 profiles were measured across two-week sampling periods from December 13<sup>th</sup> 2011 to  
180 January 9<sup>th</sup> 2013, except when weekly measurements were conducted from June 19<sup>th</sup> to  
181 August 30<sup>th</sup> 2012 when higher concentrations were anticipated. Passive samplers were  
182 prepared in an ammonia-free laminar flow hood (Envirco Corporation) and sealed for  
183 transport to the field. More detailed information regarding sampler preparation can be  
184 obtained in Day et al. (2012).

185

186 The ambient NH<sub>3</sub> concentration was calculated based on the characteristics of the passive  
187 sampler and the diffusivity of NH<sub>3</sub> in the atmosphere ( $D_{\text{NH}_3}$ ), which is a function of local  
188 temperature (T) and ambient pressure (P), and can be expressed using Eq. 1:

189 
$$D_{\text{NH}_3}(T, P) = D_{0,1} \times \left(\frac{P_0}{P}\right) \times \left(\frac{T}{T_0}\right)^{1.81} \quad (\text{Eq. 1})$$

190 where  $D_{0,1} = 0.1978 \text{ cm}^2\text{s}^{-1}$  at  $T_0 = 273 \text{ K}$  (0 °C) and  $P_0 = 1 \text{ atm}$  (Massman, 1998). Then,  
191 the diffusional flow rate through the NH<sub>3</sub> passive sampler ( $Q_{\text{NH}_3}$ ) is given by Eq. 2:

192 
$$Q_{\text{NH}_3} = D_{\text{NH}_3}(T, P) \times \frac{A}{\Delta X} \quad (\text{Eq. 2})$$

193 where  $A$  is the passive sampler effective cross-sectional area and  $\Delta X$  is the passive sampler  
194 diffusion distance. For the Radiello NH<sub>3</sub> passive sampler,  $A/\Delta X$  represents the geometric  
195 constant for radial flow and has been reported to be 14.2 cm, based on actual physical  
196 measurements (Day et al., 2012; Puchalski et al., 2011), which differs from the  
197 manufacturer's description ([http://www.radiello.com/english/nh3\\_en.htm](http://www.radiello.com/english/nh3_en.htm)). Finally, the  
198 NH<sub>3</sub> concentration in the air ( $C_{\text{NH}_3}$ ) is calculated from the diffusional flow rate ( $Q_{\text{NH}_3}$ ), the  
199 duration of sampling time ( $t$ ) and the mass of NH<sub>3</sub> collected on the cartridge ( $m_{\text{NH}_3}$ ) as  
200 shown in Eq. 3:



$$C_{NH_3} = \frac{m_{NH_3}}{t \times Q_{NH_3}} \quad (\text{Eq. 3})$$

201  
202 For the northeastern plains network, hourly temperature data were obtained from nearby  
203 CoAGMET weather stations (<http://www.coagmet.com/>) (Table S1). The average  
204 meteorological record was fairly consistent from year-to-year. The ambient pressure was  
205 calculated based on the elevation of each site. At the BAO tower, temperature and relative  
206 humidity were measured by battery-powered sensors (EBI20-TH1, EBRO Inc. Ingolstadt,  
207 Germany; <http://shop.ebro.com/chemistry/ebi-20-th.html>) co-located with the NH<sub>3</sub> passive  
208 samplers at each sampling height.

209

### 210 2.2.2 URG denuder/filter-pack sampler

211

212 During the same sampling periods as the NH<sub>3</sub> passive samplers, URG denuder/filter-pack  
213 sampling systems were also installed during select campaign years at the FC\_W, GY, and  
214 BAO tower sites to measure the concentrations of gaseous NH<sub>3</sub> and HNO<sub>3</sub>, as well as fine  
215 particulate inorganic ions. Air was drawn first through a Teflon-coated PM<sub>2.5</sub> cyclone  
216 ( $D_{50}=2.5 \mu\text{m}$ ) at the inlet, followed by two annular denuders connected in series. The first  
217 denuder was coated with sodium carbonate (Na<sub>2</sub>CO<sub>3</sub>) solution (10 g of Na<sub>2</sub>CO<sub>3</sub> and 10 g  
218 of glycerol dissolved in 500 ml of deionized water (18.2 Mohm-cm) and 500 ml methanol)  
219 to collect gaseous HNO<sub>3</sub> and sulfur dioxide (SO<sub>2</sub>). The second denuder was coated with a  
220 phosphorous acid (H<sub>3</sub>PO<sub>3</sub>) solution (10 g of H<sub>3</sub>PO<sub>3</sub> dissolved in 100 ml of deionized water  
221 and 900 ml methanol) to collect gaseous NH<sub>3</sub> in the atmosphere. The air was then drawn  
222 through a filter pack containing a 47-mm nylon filter (Nylasorb, pore size 1  $\mu\text{m}$ , Pall  
223 Corporation) to collect fine particles, followed by a backup H<sub>3</sub>PO<sub>3</sub>-coated denuder to



224 capture any  $\text{NH}_3$  re-volatilized from  $\text{NH}_4^+$  salt particles collected on the nylon filter. The  
225 URG samplers were changed at the same time as the passive samplers during each site visit.  
226 The air flow rate was controlled by a URG mass flow-controlled pump; the total flow rate  
227 through the system was nominally 3 L/min both at FC\_W, GY, and BAO. The URG  
228 sampling system has been used widely in previous studies because of its good performance  
229 in sampling gases and particles (Bari et al., 2003; Beem et al., 2010; Benedict et al.,  
230 2013a; Lee et al., 2008; Li et al., 2014; Lin et al., 2006) and was used as a reference method  
231 for evaluating the performance of the  $\text{NH}_3$  passive samplers.

232

### 233 **2.2.3 Sample analysis and evaluation**

234

235 Passive samplers and URG denuders were extracted on arrival in the lab at Colorado State  
236 University (CSU). The URG denuders were extracted with 10 ml deionized water; the  
237 Nylon filters and passive sampler cartridges were ultrasonically extracted for 55 minutes  
238 in 6 ml and 10 ml deionized water, respectively. Passive sampler and  $\text{H}_3\text{PO}_3$ -coated-  
239 denuder extracts were analyzed by ion chromatography for  $\text{NH}_4^+$ ,  $\text{Na}_2\text{CO}_3$ -coated denuder  
240 extracts were analyzed for  $\text{NO}_3^-$  and  $\text{SO}_4^{2-}$ , and all filter extracts were analyzed for cations  
241 ( $\text{Na}^+$ ,  $\text{NH}_4^+$ ,  $\text{K}^+$ ,  $\text{Mg}^{2+}$  and  $\text{Ca}^{2+}$ ) and anions ( $\text{Cl}^-$ ,  $\text{NO}_3^-$ ,  $\text{SO}_4^{2-}$ ). Cations in the samples were  
242 separated with a 20 mM methanesulfonic acid eluent (0.5 ml/min) on a Dionex CS12A  
243 column configured with a CSRS ULTRA II suppressor and detected using a Dionex  
244 conductivity detector. Anions in the samples were separated with an 8 mM carbonate/1mM  
245 bicarbonate eluent (1 ml/min) on a Dionex AS14A column followed by an ASRS ULTRA  
246 II suppressor and detected using a Dionex conductivity detector (Li et al., 2014).



247

248 Replicate Radiello passive samples were collected at FC\_W (2011, weekly), BH (2012,  
249 2013 and 2014, weekly), GY (2014, weekly and 2015, bi-weekly), KY (2014, weekly) and  
250 three different heights (1 m, 100 m and 300 m) of the BAO tower (biweekly; weekly in  
251 summer) during the campaign to evaluate the performance of NH<sub>3</sub> passive samplers under  
252 different NH<sub>3</sub> concentrations and sampling periods. Comparison of replicate samples  
253 yielded good precision (see Fig. S1) with a pooled relative standard deviation of 8.9%. The  
254 weekly and biweekly NH<sub>3</sub> concentrations collected by passive samplers were also in good  
255 agreement with measurements by co-located URG denuder samplers for the same sampling  
256 durations (a linear least-squares regression fit yielded a correlation coefficient (R<sup>2</sup>) between  
257 the two methods of 0.92 with a slope of 0.98 and a small positive intercept (0.25 µg/m<sup>3</sup>;  
258 Fig. S2). These findings are consistent with previous studies (Benedict et al., 2013a; Day et  
259 al., 2012; Puchalski et al., 2011). Field and laboratory blanks were collected throughout the  
260 research campaign and used to blank correct sample results and determine the minimum  
261 detection limits (MDL). From the field blanks, the MDL was calculated to be 0.27 µg/m<sup>3</sup>  
262 for a one-week Radiello passive NH<sub>3</sub> sample.

263

### 264 **2.3 Satellite retrievals of ammonia**

265

266 The Infrared Atmospheric Sounding Interferometer (IASI) is a passive infrared Fourier  
267 transform spectrometer onboard the MetOp platforms, operating in nadir (Clerbaux et al.,  
268 2009). IASI provides a quasi-global coverage twice a day with overpass times at around  
269 9:30 am and 9:30 pm (when crossing the equator) at a relatively small pixel size (circle



270 with 12 km diameter at nadir, distorted to ellipse-shaped pixels off-nadir). The combination  
271 of low instrumental noise ( $\sim 0.2$  K at  $950\text{ cm}^{-1}$  and 280 K), a medium spectral resolution  
272 ( $0.5\text{ cm}^{-1}$  apodized) and a continuous spectral coverage between  $645$  and  $2760\text{ cm}^{-1}$  makes  
273 IASI a suitable instrument to measure various constituents of the atmosphere (Clarisse et  
274 al., 2011).

275

276 The IASI-NH<sub>3</sub> data set used in this work is based on a recently developed retrieval scheme  
277 presented in detail in Whitburn et al. (2016). The first step of the retrieval scheme is to  
278 calculate a so-called Hyperspectral Range Index (HRI) for each IASI spectrum, which is  
279 representative of the amount of NH<sub>3</sub>. This HRI is subsequently converted into NH<sub>3</sub> total  
280 columns using a neural network (NN) approach. It is an extension of the HRI method  
281 presented in Van Damme et al. (2014a) who used two-dimensional look-up tables (LUTs)  
282 for the radiance-concentration conversion. The new NN-based method inherits the  
283 advantages of the LUT-based HRI method whilst providing several significant  
284 improvements (Whitburn et al., 2016).

285

### 286 **3 Results and discussion**

#### 287 **3.1 Spatial distributions of NH<sub>3</sub>**

288

289 Large spatial differences in NH<sub>3</sub> concentrations were found in the northeastern plains of  
290 Colorado with mean NH<sub>3</sub> concentrations ranging from  $2.66\text{ }\mu\text{g/m}^3$  to  $42.7\text{ }\mu\text{g/m}^3$  as  
291 illustrated in Fig. 1. Also included in Fig. 1 are, for qualitative comparisons, estimated NH<sub>3</sub>  
292 emissions from major feedlots in northeastern Colorado. The feedlots were classified into



293 categories based on the type of animals raised (data were provided by the Colorado  
294 Department of Public Health and Environment) and NH<sub>3</sub> emissions were calculated  
295 following Eq. 4:

$$296 \quad \text{NH}_3 \text{ Emission} = \sum (\text{Population} \times \text{Emission Factor}) \quad (\text{Eq. 4})$$

297 where the NH<sub>3</sub> emissions are the total NH<sub>3</sub> emitted from each feedlot in tons per year  
298 (converted from kg to tons for Fig. 1). Population is the animal population in each feedlot  
299 and the emission factor was specified for each kind of animal: 44.3, 38.1, 3.37, 0.27, 6.50  
300 and 12.2 kg NH<sub>3</sub>/head/year, for beef cattle, dairy cows, sheep, poultry, swine and horses,  
301 respectively (USEPA, 2004; Todd et al., 2013). 73% of the total regional feedlot emissions  
302 are contributed by beef feedlots. Many large sources are located within several tens of km  
303 to the south, east, and north of Greeley. Other large sources are located further east along  
304 the South Platte River with some smaller sources (mostly dairies) located further west in  
305 the sampling region, closer to the urban corridor.

306

307 The lowest average ambient NH<sub>3</sub> concentrations in the sampling network were found at  
308 remote grassland sites such as NN and BE: 2.66 μg/m<sup>3</sup> and 3.07 μg/m<sup>3</sup>, respectively.  
309 Concentrations of NH<sub>3</sub> at suburban sites were somewhat higher than at these remote, rural  
310 sites, indicating possible impacts of human activities such as emissions from vehicles  
311 equipped with three-way catalytic converters, local waste treatment, and fertilization of  
312 yards and parks on local NH<sub>3</sub> concentrations. The measured weekly average NH<sub>3</sub>  
313 concentration at the Loveland golf course (GC) site was 5.14 μg/m<sup>3</sup> with a range of 1.81  
314 μg/m<sup>3</sup> to 7.87 μg/m<sup>3</sup>, showing only slightly elevated values compared to NH<sub>3</sub>  
315 concentrations at other nearby suburban sites (FC\_W and LD) suggesting that golf course



316 fertilization at this location is probably not a major, regional NH<sub>3</sub> source. The highest  
317 ambient NH<sub>3</sub> concentrations were consistently observed at sites near extensive animal  
318 feeding operations. Compared to the remote sites (NN and BE), an approximately 2-5 fold  
319 increase in NH<sub>3</sub> concentrations was observed at BH and AT (6.17 and 13.8 μg/m<sup>3</sup>), rural  
320 sites under the influence of nearby animal feeding operation emissions. A 15-fold increase  
321 in NH<sub>3</sub> concentrations was observed from the grassland NN and BE sites (2.66 and 3.07  
322 μg/m<sup>3</sup>) to KY (42.73 μg/m<sup>3</sup>), 0.4 km from a feedlot with almost 100,000 cattle.

323

324 The average summertime NH<sub>3</sub> concentrations sampled at each site spanning several years  
325 exhibited a statistically significant (p<0.1) inter-annual trend (Fig. 2), at three sites; six  
326 sites showed no significant trend. Both the GY and KY sites show increasing trends, while  
327 BH exhibits a decreasing trend. Trend analysis was conducted using Theil regression (Theil,  
328 1992) and the Mann-Kendall test (Gilbert, 1987;Marchetto et al., 2013). We define an  
329 increasing (decreasing) trend as a positive (negative) slope of the Theil regression, while  
330 the statistical significance of a trend was determined by the Mann-Kendall test (p-value).  
331 A 90<sup>th</sup> percentile significance level (p<0.10) was assumed as in a previous study (Hand et  
332 al., 2012). The power of these analyses are limited by the relatively small number of  
333 measurement years to date; additional power for assessing interannual trends will become  
334 available as the measurement record lengthens. Data from the Colorado Agricultural  
335 Statistics Report (2014,  
336 [http://www.nass.usda.gov/Statistics\\_by\\_State/Colorado/Publications/Annual\\_Statistical\\_Bulletin/Bulletin2015.pdf](http://www.nass.usda.gov/Statistics_by_State/Colorado/Publications/Annual_Statistical_Bulletin/Bulletin2015.pdf)) indicate that Weld, Larimer, and Morgan counties (three major  
337 counties located in the northeastern plains of Colorado) did not show significant growth in  
338



339 livestock numbers between 2009 and 2014. The total annual numbers of beef cattle, milk  
340 cows, cattle and calves in these counties were 986, 974, 996, 1065, 955 and 936 thousand  
341 head, respectively, in the six years from 2009 to 2014.

342

343 A number of best management practices (BMPs) are under evaluation to help agricultural  
344 producers in the region to lower  $\text{NH}_3$  emissions as part of efforts to reduce reactive nitrogen  
345 deposition in Rocky Mountain National Park. The baseline regional concentration  
346 information gathered here will be critical in helping to evaluate the success of future efforts  
347 to reduce  $\text{NH}_3$  emissions.

348

349 Weekly average atmospheric  $\text{NH}_3$  concentrations at each observation site are plotted for  
350 summers 2010-2015 in Fig. 3. These observations again show the general similarity, at a  
351 given location, of summertime concentrations across several years. Some variation from  
352 week to week is expected due to differences in meteorology. Emissions, for example, are  
353 dependent on the temperature, dispersion is influenced by turbulence and mixing layer  
354 depth, and removal is influenced by precipitation and turbulence. One clear outlier period  
355 is the elevated  $\text{NH}_3$  concentrations observed at FC\_W at the beginning of summer 2012  
356 (Fig. 3c). The maximum weekly average  $\text{NH}_3$  concentration at this site ( $8.55 \mu\text{g}/\text{m}^3$ ) was  
357 measured during June 21-28, 2012 and was more than two times the average  $\text{NH}_3$   
358 concentration in 2010 ( $4.13 \mu\text{g}/\text{m}^3$ ) and 2011 ( $3.76 \mu\text{g}/\text{m}^3$ ) (see Table 2). This is supported  
359 by the satellite observation reported by IASI (see Section 3.3 and Figure 7). During this  
360 elevated concentration period, the High Park Fire, one of the largest fires recorded in  
361 Colorado history at  $353 \text{ km}^2$  burned, was burning in the mountains west of Fort Collins



362 and the city was frequently impacted by smoke. The fire was first spotted on June 9, 2012  
363 and declared 100% contained on June 30, 2012  
364 ([http://en.wikipedia.org/wiki/High\\_Park\\_fire](http://en.wikipedia.org/wiki/High_Park_fire)). During the wildfire period, on-line  
365 instruments (Picarro NH<sub>3</sub> analyzer and Teledyne CO analyzer) were also set up to measure  
366 CO and NH<sub>3</sub> concentrations near the FC\_W site. A significant correlation between CO and  
367 NH<sub>3</sub> was found during the wildfire (Prenni et al., 2012;Benedict et al., 2017). Elevated NH<sub>3</sub>  
368 concentrations in the High Park Fire plume are evidence of the importance of wild and  
369 prescribed burning as a source of atmospheric NH<sub>3</sub>, reinforcing similar findings from  
370 previous studies (Coheur et al., 2009;Prenni et al., 2014;Sutton et al., 2000;Whitburn et al.,  
371 2015).

372

### 373 **3.2 Vertical distribution of NH<sub>3</sub>**

374

375 While surface measurements of NH<sub>3</sub> concentrations remain uncommon, measurements of  
376 vertical profiles of NH<sub>3</sub> concentrations above the surface are extremely rare. Time series  
377 of vertical profiles of ambient NH<sub>3</sub> concentrations measured at the BAO tower across the  
378 full year of 2012 are shown in Fig. 4. During most sampling periods, the NH<sub>3</sub> concentration  
379 exhibited a maximum at 10 m decreasing both toward the lowest (1 m) measurement point  
380 and with height above 10 m. The minimum concentration was observed at the highest  
381 measurement point at the top (300 m) of the BAO tower. While the major sources of NH<sub>3</sub>  
382 are surface emissions, it is not surprising to see a gradient of decreasing concentration near  
383 the surface at this location where local emissions are expected to be small and the net local  
384 flux represents surface deposition (Pul et al., 2009). The long time between successive



385 passive measurements (1-2 weeks) in this study precludes a meaningful determination of  
386 surface removal rates based on the observed concentration gradient.

387

388 Seasonal variations in the vertical profile of  $\text{NH}_3$  are depicted in Fig. 5 with March, April  
389 and May defined as spring; June, July and August as summer; September, October and  
390 November as fall; and December, January and February as winter. Vertical concentration  
391 differences were greatest in winter (from an average concentration greater than  $4 \mu\text{g}/\text{m}^3$   
392 near the surface to approximately  $1 \mu\text{g}/\text{m}^3$  at 300 m, representing a decrease of  
393 approximately 75%) followed by fall. Low level temperature inversions which trap  
394 emissions closer to the surface are common in both seasons (fall and winter). The highest  
395 concentrations across the profile were observed in summer, when emissions increase due  
396 to higher temperatures and vertical mixing is enhanced. The concentration decrease from  
397 the surface to 300 m average only 44% in summer. Increased  $\text{NH}_3$  concentrations in  
398 summer also may reflect a shift in thermodynamic equilibrium of particulate  $\text{NH}_4\text{NO}_3$   
399 toward its gas phase precursors  $\text{NH}_3$  and  $\text{HNO}_3$ . Previous studies have reported increased  
400  $\text{NH}_3$  concentrations in summer and/or reduced concentrations in winter due to the seasonal  
401 changes of  $\text{NH}_3$  emissions and gas-particle partitioning (Li et al., 2014; Meng et al.,  
402 2011; Plessow et al., 2005; Walker et al., 2004; Zbieranowski and Aherne, 2012). Day et al.  
403 (2012) previously suggested that trapping of regional  $\text{NH}_3$  emissions in a shallow winter  
404 boundary layer can produce elevated surface concentrations. The BAO tower observations  
405 in Fig. 5a support this hypothesis, as concentrations are elevated near the surface but fall  
406 off quickly at heights greater than 10-20 m. Evidence of winter temperature inversions is  
407 present even in the average winter temperature profile shown in Fig. 5b.



408

409 Several long-term measurements have shown a strong correlation between NH<sub>3</sub>  
410 concentrations and ambient temperature, due to enhanced NH<sub>3</sub> emissions from soil and  
411 volatilization from NH<sub>4</sub>NO<sub>3</sub> particulate matter (Bari et al., 2003; Ianniello et al., 2010; Lin  
412 et al., 2006; Meng et al., 2011). Almost no correlation ( $R^2 = 0.02$ ) between NH<sub>3</sub> and  
413 temperature was observed at 1 m height in the current study; higher correlation ( $R^2 = 0.65$ )  
414 was found at the top of the tower (Fig. S3a). The correlation coefficients increase  
415 substantially with height (Fig. S3b), particularly above 50 m, suggesting that temperature  
416 might influence ambient NH<sub>3</sub> concentrations at this location at higher altitude but is not a  
417 dominant factor at the surface (Fig. S3b). This pattern likely reflects greater vertical mixing  
418 during warmer periods, as discussed above. In order to investigate the possible influence  
419 of changes in NH<sub>4</sub>NO<sub>3</sub> aerosol-gas partitioning on vertical NH<sub>3</sub> concentration profiles,  
420 thermodynamic simulations were performed using the ISORROPIA II model (Fountoukis  
421 and Nenes, 2007) (Fig. S4). Model inputs included BAO site URG denuder/filter-pack  
422 surface measurements of key species (gaseous NH<sub>3</sub> and HNO<sub>3</sub> and PM<sub>2.5</sub> NH<sub>4</sub><sup>+</sup>, NO<sub>3</sub><sup>-</sup>, and  
423 SO<sub>4</sub><sup>2-</sup>) and measurements of temperature and relative humidity at each tower measurement  
424 height. Because vertical differences in temperature and relative humidity were generally  
425 small, little change was predicted with height in the thermodynamic partitioning of the  
426 NH<sub>3</sub>-HNO<sub>3</sub>-NH<sub>4</sub>NO<sub>3</sub> system. Consequently, a shift in partitioning toward the particle  
427 phase as temperatures cool at higher altitudes appears not to account for much of the  
428 observed decrease in NH<sub>3</sub> concentration with height. For this location and for the lowest  
429 300 m of the atmosphere, the vertical thermal structure of the atmosphere and associated



430 mixing, ambient dilution, and  $\text{NH}_3$  surface deposition appear to be the major factors  
431 determining vertical distributions of atmospheric  $\text{NH}_3$ .

432

### 433 **3.3 Comparison with Satellite Observations**

434

435 Several recent studies have used surface  $\text{NH}_3$  measurements to evaluate or improve remote  
436 sensing techniques for retrieving  $\text{NH}_3$  concentrations and determining distributions (Heald  
437 et al., 2012; Pinder et al., 2011; Zhu et al., 2013; Van Damme et al., 2015). The first version  
438 of the IASI- $\text{NH}_3$  data set has been evaluated against model simulations over Europe and  
439 has shown its consistency (Van Damme et al., 2014). These initial validation steps  
440 highlighted the need to expand the  $\text{NH}_3$  monitoring network to achieve a more complete  
441 validation of the  $\text{NH}_3$  satellite observations (Van Damme et al., 2015). The comparison  
442 here is a contribution to that effort and benefits from a relatively high spatial density of  
443 monitoring sites in a region with substantial ammonia emission and concentration gradients.

444

445 In Fig. 6 IASI-retrieved column distributions averaged over the ground-based  
446 measurement period from 2012 to 2015 are compared with the Radiello passive  $\text{NH}_3$   
447 surface concentration measurements in northeastern Colorado. Only IASI observations  
448 with a relative error below 100% or an absolute error below  $5 \times 10^{15}$  molec/cm<sup>2</sup> were  
449 considered for comparison in the latitude range from 39.75°N to 41.0°N and longitude  
450 range from 103.4°W to 105.3°W. Overall, the IASI observations and Radiello passive  
451 measurements show similar spatial patterns. The IASI columns exceed  $2 \times 10^{16}$  molec/cm<sup>2</sup>  
452 around the KY site and decrease moving away from concentrated agricultural areas.



453

454 In order to further explore the temporal concentration variability, including the postulated  
455 contributions from wildfire to local ambient NH<sub>3</sub> concentrations, averages of IASI  
456 measurements (based on weekly or bi-weekly Radiello passive sampling periods) above  
457 the FC\_W site are shown in Fig. 7. In general, similar temporal trends are found between  
458 the Radiello passive measurements (blue) and IASI observations (red). Elevated NH<sub>3</sub>  
459 concentrations during the High Park Fire period in June 2012 are seen in both the satellite  
460 and surface measurements. It is also interesting to note the relatively high IASI-NH<sub>3</sub> total  
461 column measured at the beginning of June 2011 ( $8.5 \times 10^{15}$  molec/cm<sup>2</sup>), which could be  
462 linked with wildfire plumes at higher altitude (Fig. S5) transported from other areas and  
463 not captured by the surface measurements.

464

465 The similar spatial and temporal patterns captured show the respective consistency of the  
466 IASI measurements and the Radiello network to monitor regional NH<sub>3</sub> variations in  
467 northeast Colorado. The passive measurements provide a good, long-term record of spatial  
468 variability and surface concentration trends while the IASI satellite NH<sub>3</sub> columns provide  
469 higher time resolution snapshots of conditions over the region, including plumes elevated  
470 above the surface.

471

### 472 **3.4 Comparison with CAMx Model Simulations**

473

474 Chemical transport models are valuable tools for evaluating how various processes  
475 influence ambient air quality and pollutant deposition. They can be especially helpful in



476 designing effective source control strategies for air quality improvement. Unfortunately,  
477 current models frequently have difficulties accurately simulating spatial concentrations of  
478  $\text{NH}_3$ . In addition to the typical model difficulties in accurately simulating transport,  $\text{NH}_3$   
479 emissions are not well constrained and the parameterization of  $\text{NH}_3$  deposition is  
480 challenging. In order to examine some of these issues, ammonia measurements from this  
481 study are compared to modeled concentrations from the Comprehensive Air quality Model  
482 with extensions (CAMx, [http://www.camx.com/files/camxusersguide\\_v6-20.pdf](http://www.camx.com/files/camxusersguide_v6-20.pdf)). CAMx,  
483 a photochemical model that simulates the emissions, transport, chemistry and removal of  
484 chemical species in the atmosphere, is one of US EPA's recommended regional chemical  
485 transport models and is frequently used for air quality analysis (EPA, 2007, 2011). The  
486 2011 modelled period presented here (version base\_2011a), including inputs representing  
487 emissions and meteorology, was developed for the Western Air Quality Data Warehouse  
488 (IWDW-WAQS, 2015); details on modeling protocol and model performance are available  
489 on the IWDW website (<http://views.cira.colostate.edu/tsdw/>).

490

491 Simulations with CAMx version 6.1 were performed with two-way nested domains with  
492 horizontal grid size resolutions of 36 km, 12 km, and 4 km (Fig. S6). The outermost domain  
493 includes the continental United States, southern Canada, and northern Mexico, the 12-km  
494 domain extends over the western states, and the 4-km domain extends over Colorado,  
495 Wyoming and Utah. The Weather Research & Forecasting Model (WRF), Advanced  
496 Research WRF (ARW) v3.5.1, was used to develop meteorological inputs to the air quality  
497 model (Skamarock et al., 2005). The input meteorological data represent conditions as they  
498 occurred in 2011. A performance evaluation of the WRF simulations was conducted by



499 The University of North Carolina at Chapel Hill (Three-State Air Quality Modeling Study  
500 (3SAQS) – Weather Research Forecast 2011 Meteorological Model  
501 Application/Evaluation available at:  
502 [http://vibe.cira.colostate.edu/wiki/Attachments/Modeling/3SAQS\\_2011\\_WRF\\_MPE\\_v05](http://vibe.cira.colostate.edu/wiki/Attachments/Modeling/3SAQS_2011_WRF_MPE_v05)  
503 Mar2015.pdf).

504

505 The Sparse Matrix Operator Kernel Emissions (SMOKE) processing system  
506 (<https://www.cmascenter.org/smoke/documentation/3.1/html/>) (Houyoux et al., 2000) was  
507 used to prepare the emissions inventory data in a format that reflects the spatial, temporal,  
508 and chemical speciation parameters required by CAMx. The emissions inventory is based  
509 on the 2011 National Emissions Inventory (NEI) v1  
510 ([http://www.epa.gov/ttn/chief/net/2011nei/2011\\_nei\\_tsdv1\\_draft2\\_june2014.pdf](http://www.epa.gov/ttn/chief/net/2011nei/2011_nei_tsdv1_draft2_june2014.pdf)).

511 Important updates to the 2011 NEI included a detailed oil and gas inventory, and the spatial  
512 allocation of livestock emissions using latitude/longitude location data of livestock  
513 facilities (IWDW-WAQS). Boundary conditions were developed using the Model for  
514 Ozone and Related chemical Tracers (MOZART) and represent the 2011 modeling period  
515 (Emmons et al., 2010).

516

517 Fig. 8 illustrates an evaluation of CAMx simulated NH<sub>3</sub> concentrations both spatially and  
518 across time. Generally speaking, CAMx reasonably reproduces average observed NH<sub>3</sub> in  
519 the northeastern plains of Colorado, with a model/measurement ratio of 91% averaged  
520 across all measurement locations. This is a much closer match than a separate 12 km  
521 resolution CMAQ summer 2014 model comparison to surface passive ammonia



522 measurements (including some of the observations collected in the current study) reported  
523 by Battye et al. (2016), who found an averaged measured concentration 2.7 times higher  
524 than the modeled concentration. Despite the better average comparison of measurements  
525 with the CAMx prediction reported here, however, the CAMx simulation tends to  
526 overestimate concentrations near major NH<sub>3</sub> sources (e.g., at the KY monitoring site),  
527 while underestimating NH<sub>3</sub> concentrations at sites further away from feedlot locations (Fig.  
528 9). Across our measurement locations, the model performance is best at GY, a site  
529 surrounded by but not immediately adjacent to large NH<sub>3</sub> sources. The modest  
530 overestimation of NH<sub>3</sub> concentration at the KY site is likely an artifact of model resolution  
531 and the assumption that emissions are immediately and homogeneously dispersed  
532 throughout the grid cell in which they are emitted. A model-measurement mismatch  
533 moving farther away from NH<sub>3</sub> source locations could result from a number of factors,  
534 including smaller and/or non-agricultural sources (e.g., suburban N-fertilization or  
535 transportation) underrepresented in the emissions inventory, possible overestimation of  
536 NH<sub>3</sub> deposition in the model, which does not account for the bidirectional nature of NH<sub>3</sub>  
537 exchange with the surface, or a tendency for the model to more actively move surface NH<sub>3</sub>  
538 emissions aloft during downwind transport than occurs in the real atmosphere.

539

540 Fig. 10a shows both measured (measurements taken in 2012) and modeled (2011) vertical  
541 concentrations of NH<sub>3</sub> at the BAO tower location. Although these comparisons are for two  
542 adjacent years, the results presented earlier demonstrate that seasonal average  
543 concentrations across the region are typically similar from year to year. Modeled vertical  
544 NH<sub>3</sub> concentrations are reported from the lowest 6 levels of the model, up to approximately



545 325 m above the surface. The model height represented by the value plotted on the y-axis  
546 in Fig. 10a represents the top of the layer from which the corresponding concentration is  
547 reported (i.e. the surface or lowest model layer is reported at 24 meters – the approximate  
548 height of the surface layer). Model layer height is based on the meteorological model and  
549 modeled pressure and is not fixed  
550 ([http://vibe.cira.colostate.edu/wiki/Attachments/Modeling/3SAQS\\_2011\\_WRF\\_MPE\\_v0\\_5Mar2015.pdf](http://vibe.cira.colostate.edu/wiki/Attachments/Modeling/3SAQS_2011_WRF_MPE_v0_5Mar2015.pdf)). The vertical concentrations are homogeneous within each model layer.  
552 Therefore, the model is not able to capture the detailed vertical pattern shown from 0 to 10  
553 to 20 meters by the observations.

554

555 The model-measurement comparisons of vertical profiles demonstrate a significant  
556 underprediction by the model at all elevations in all four seasons. The underprediction at  
557 the surface is consistent with the observation above that the model tends to underestimate  
558 ammonia concentrations farther from the major regional feedlot sources. The fact that the  
559 model also underpredicts ammonia aloft suggests that the surface mismatch is not simply  
560 a result of excess vertical transport of ammonia in the model. Model vertical  $\text{NH}_3$   
561 concentration profiles normalized for surface concentration are shown in Fig. 10b and  
562 compared to similarly normalized measurements. These profiles suggest that the model  
563 does a fairly reasonable job of capturing the shape of the observed vertical concentration  
564 gradient, although the relative concentration decrease with height in the model is a bit  
565 stronger than observed in each season.

566

567 **4 Conclusions**



568

569 Six years of observed NH<sub>3</sub> concentrations revealed strong spatial differences in NH<sub>3</sub>  
570 concentrations in northeastern Colorado. Summer average weekly NH<sub>3</sub> concentrations  
571 ranged from 2.7 µg/m<sup>3</sup> to 42.7 µg/m<sup>3</sup>. The lowest average NH<sub>3</sub> concentration always  
572 occurred at a remote prairie site, while average NH<sub>3</sub> concentrations nearly a factor of 15  
573 greater were observed at a site near a large animal feeding operation. Based on six years of  
574 available data, no significant regional long-term trends were detected in NH<sub>3</sub>  
575 concentrations at 6 of the 9 study sites, consistent with similar seasonal meteorological  
576 conditions and relative stability in regional livestock headcounts over the period. Two sites  
577 near animal feeding operations (GY and KY) showed evidence of an increasing NH<sub>3</sub>  
578 concentration trend, while a decreasing trend was evident at a 3<sup>rd</sup> site. Further effort is  
579 warranted to see whether changes in local animal feeding operations might explain these  
580 trends. The NH<sub>3</sub> concentration levels observed in this study provide an important reference  
581 point for evaluating the success of future efforts to mitigate regional NH<sub>3</sub> emissions  
582 through voluntary implementation of BMPs as part of a strategy to reduce nitrogen  
583 deposition levels and impacts in nearby Rocky Mountain National Park.

584

585 Measurement of NH<sub>3</sub> at the BAO meteorological tower near Erie, Colorado provide the  
586 first long-term insights into vertical gradients of NH<sub>3</sub> concentrations in the region and some  
587 of the first long-term measurements of this type anywhere in the world. A general pattern  
588 of decreased NH<sub>3</sub> concentrations with height above 10 m was observed in all seasons as  
589 was a decrease in concentration below 10 m height. Moderate average concentrations were  
590 observed in winter at the surface along with a steeper vertical concentration gradient.



591 Higher average concentrations were observed in summer at all altitudes along with a  
592 shallower vertical concentration gradient. Surface deposition, vertical dilution, and the  
593 formation of thermal inversions that limit the vertical mixing of regional, surface-based  
594 NH<sub>3</sub> emissions appear to have greater influence than temperature and humidity-driven  
595 changes in NH<sub>4</sub>NO<sub>3</sub> gas-particle partitioning on the observed vertical concentration  
596 profiles.

597

598 Comparison of measured NH<sub>3</sub> spatial distributions with IASI satellite retrieved NH<sub>3</sub>  
599 columns reveals both monitoring techniques capture similar spatial and temporal  
600 variability in northeastern Colorado. These comparisons lend additional weight to the  
601 growing body of evidence suggesting that satellite retrievals of NH<sub>3</sub> columns can provide  
602 useful information about spatial and temporal concentration variability of this key species,  
603 even in regions with strong sources and sharp spatial concentration gradients. Some  
604 temporal differences between satellite and in situ measurements at the FC\_W site appear  
605 to reflect NH<sub>3</sub> in elevated wildfire plumes that are observed from the satellite but are not  
606 sampled at the surface.

607

608 Measured spatial distributions of NH<sub>3</sub> concentrations also provide a good basis for  
609 comparison to regional air quality model simulations. A comparison with CAMx  
610 simulations finds that the model does a good job capturing average ammonia  
611 concentrations across the study, but tends to overpredict concentrations close to sources  
612 and underpredict concentrations at locations further away. A comparison of measured and  
613 modeled vertical profiles in a non-source region reveals an underprediction of modeled



614 ammonia from the surface up to 300 m in all seasons. The mismatch aloft provides evidence  
615 that the difficulty the model has reproducing surface observations away from sources is not  
616 a simple result of excess vertical mixing of ammonia emissions in the model. Rather, the  
617 model emission inventory may be missing or underpredicting smaller or non-agricultural  
618 ammonia sources or, perhaps more likely, the model may be overpredicting surface  
619 ammonia deposition due to the absence of bidirectional treatment of ammonia atmosphere-  
620 surface exchange. Although additional research is definitely needed, we expect the NH<sub>3</sub>  
621 concentrations and spatial/vertical differences presented here to be useful in constraining  
622 future simulated concentrations of atmospheric NH<sub>3</sub> in chemical transport models.

623

#### 624 **Acknowledgements**

625

626 Primary funding for this work was provided by the USDA through the Colorado State  
627 University Agriculture Experiment Station (project COL00699). Additional support and  
628 equipment were provided by the National Park Service. The authors are grateful to the  
629 many people who helped to make these measurements possible, especially allowing access  
630 to the sampling sites. The authors thank Bonne Ford, Arsineh Hecobian and Liye Zhu from  
631 Colorado State University for their helpful suggestions. The authors thank Daniel Wolfe  
632 and Bruce Bartram from the BAO tower for assistance with the tower measurements. The  
633 authors also thank Tom Moore from Western States Air Resources Council and Rodger  
634 Ames from Cooperative Institute for Research in the Atmosphere for modeling help. S. W.  
635 is grateful for his Ph.D. grant (Boursier FRIA) to the “Fonds pour la Formation à la  
636 Recherche dans l’Industrie et dans l’Agriculture” of Belgium. L. C. is a Research Associate



637 (Chercheur Qualifié) with the Belgian F.R.S.-FNRS. The data included in this paper are  
638 maintained at Colorado State University and will be available for a minimum of 5 years  
639 after publication by contacting [collett@atmos.colostate.edu](mailto:collett@atmos.colostate.edu).



640 **Reference**

- 641 Aneja, V. P., Roelle, P. A., Murray, G. C., Southerland, J., Erisman, J. W., Fowler, D.,  
642 Asman, W. A. H., and Patni, N.: Atmospheric nitrogen compounds II: emissions,  
643 transport, transformation, deposition and assessment, Atmospheric Environment,  
644 35, 1903-1911, [http://dx.doi.org/10.1016/S1352-2310\(00\)00543-4](http://dx.doi.org/10.1016/S1352-2310(00)00543-4), 2001.
- 645 Aneja, V. P., Schlesinger, W. H., Nyogi, D., Jennings, G., Gilliam, W., Knighton, R. E.,  
646 Duke, C. S., Blunden, J., and Krishnan, S.: Emerging national research needs for  
647 agricultural air quality, Eos, Transactions American Geophysical Union, 87, 25-29,  
648 10.1029/2006EO030001, 2006.
- 649 Asman, W. A. H., Sutton, M. A., and SchjØRring, J. K.: Ammonia: emission, atmospheric  
650 transport and deposition, New Phytologist, 139, 27-48, 10.1046/j.1469-  
651 8137.1998.00180.x, 1998.
- 652 Bari, A., Ferraro, V., Wilson, L. R., Luttinger, D., and Husain, L.: Measurements of  
653 gaseous HONO, HNO<sub>3</sub>, SO<sub>2</sub>, HCl, NH<sub>3</sub>, particulate sulfate and PM<sub>2.5</sub> in New York,  
654 NY, Atmospheric Environment, 37, 2825-2835, [http://dx.doi.org/10.1016/S1352-  
655 2310\(03\)00199-7](http://dx.doi.org/10.1016/S1352-2310(03)00199-7), 2003.
- 656 Battye, W. H., Bray, C. D., Aneja, V. P., Tong, D., Lee, P., and Tang, Y.: Evaluating  
657 ammonia (NH<sub>3</sub>) predictions in the NOAA National Air Quality Forecast Capability  
658 (NAQFC) using in situ aircraft, ground-level, and satellite measurements from the  
659 DISCOVER-AQ Colorado campaign, Atmospheric Environment, 140, 342-351,  
660 <http://dx.doi.org/10.1016/j.atmosenv.2016.06.021>, 2016.



- 661 Bauer, S. E., Tsigaridis, K., and Miller, R.: Significant atmospheric aerosol pollution  
662 caused by world food cultivation, *Geophysical Research Letters*, 43, 5394-5400,  
663 10.1002/2016GL068354, 2016.
- 664 Beem, K. B., Raja, S., Schwandner, F. M., Taylor, C., Lee, T., Sullivan, A. P., Carrico, C.  
665 M., McMeeking, G. R., Day, D., and Levin, E.: Deposition of reactive nitrogen  
666 during the Rocky Mountain Airborne Nitrogen and Sulfur (RoMANS) study,  
667 *Environmental Pollution*, 158, 862-872, 2010.
- 668 Benedict, K. B., Chen, X., Sullivan, A. P., Li, Y., Day, D., Prenni, A. J., Levin, E.,  
669 Kreidenweis, S. M., Malm, W. C., and Schichtel, B. A.: Atmospheric  
670 concentrations and deposition of reactive nitrogen in Grand Teton National Park,  
671 *Journal of Geophysical Research: Atmospheres*, 118, 11,875-811,887, 2013a.
- 672 Benedict, K. B., Day, D., Schwandner, F. M., Kreidenweis, S. M., Schichtel, B., Malm, W.  
673 C., and Collett, J. L.: Observations of atmospheric reactive nitrogen species in  
674 Rocky Mountain National Park and across northern Colorado, *Atmospheric  
675 Environment*, 64, 66-76, 10.1016/j.atmosenv.2012.08.066, 2013b.
- 676 Benedict, K. B., Prenni, A. J., Carrico, C. M., Sullivan, A. P., Schichtel, B. A., and Collett  
677 Jr, J. L.: Enhanced concentrations of reactive nitrogen species in wildfire smoke,  
678 *Atmospheric Environment*, 148, 8-15,  
679 <http://dx.doi.org/10.1016/j.atmosenv.2016.10.030>, 2017.
- 680 Cisneros, R., Bytnerowicz, A., Schweizer, D., Zhong, S., Traina, S., and Bennett, D. H.:  
681 Ozone, nitric acid, and ammonia air pollution is unhealthy for people and  
682 ecosystems in southern Sierra Nevada, California, *Environmental Pollution*, 158,  
683 3261-3271, <http://dx.doi.org/10.1016/j.envpol.2010.07.025>, 2010.



- 684 Clarisse, L., R'Honi, Y., Coheur, P.-F., Hurtmans, D., and Clerbaux, C.: Thermal infrared  
685 nadir observations of 24 atmospheric gases, *Geophysical Research Letters*, 38,  
686 L10802, 10.1029/2011GL047271, 2011.
- 687 Clerbaux, C., Boynard, A., Clarisse, L., George, M., Hadji-Lazaro, J., Herbin, H.,  
688 Hurtmans, D., Pommier, M., Razavi, A., and Turquety, S.: Monitoring of  
689 atmospheric composition using the thermal infrared IASI/MetOp sounder,  
690 *Atmospheric Chemistry and Physics*, 9, 6041-6054, 2009.
- 691 Coheur, P.-F., Clarisse, L., Turquety, S., Hurtmans, D., and Clerbaux, C.: IASI  
692 measurements of reactive trace species in biomass burning plumes, *Atmospheric*  
693 *Chemistry and Physics*, 9, 5655-5667, 2009.
- 694 Davidson, C. I., Phalen, R. F., and Solomon, P. A.: Airborne Particulate Matter and Human  
695 Health: A Review, *Aerosol Science and Technology*, 39, 737-749,  
696 10.1080/02786820500191348, 2005.
- 697 Day, D. E., Chen, X., Gebhart, K. A., Carrico, C. M., Schwandner, F. M., Benedict, K. B.,  
698 Schichtel, B. A., and Collett, J. L.: Spatial and temporal variability of ammonia and  
699 other inorganic aerosol species, *Atmospheric Environment*, 61, 490-498,  
700 10.1016/j.atmosenv.2012.06.045, 2012.
- 701 Eilerman, S. J., Peischl, J., Neuman, J. A., Ryerson, T. B., Aikin, K. C., Holloway, M. W.,  
702 Zondlo, M. A., Golston, L. M., Pan, D., Floerchinger, C., and Herndon, S. C.:  
703 Characterization of ammonia, methane, and nitrous oxide emissions from  
704 concentrated animal feeding operations in northeastern Colorado, *Environmental*  
705 *Science & Technology*, 10.1021/acs.est.6b02851, 2016.



- 706 Ellis, R. A., Jacob, D. J., Sulprizio, M. P., Zhang, L., Holmes, C. D., Schichtel, B. A., Blett,  
707 T., Porter, E., Pardo, L. H., and Lynch, J. A.: Present and future nitrogen deposition  
708 to national parks in the United States: critical load exceedances, Atmospheric  
709 Chemistry and Physics, 13, 9083-9095, 10.5194/acp-13-9083-2013, 2013.
- 710 Emmons, L., Walters, S., Hess, P., Lamarque, J.-F., Pfister, G., Fillmore, D., Granier, C.,  
711 Guenther, A., Kinnison, D., and Laepple, T.: Description and evaluation of the  
712 Model for Ozone and Related chemical Tracers, version 4 (MOZART-4),  
713 Geoscientific Model Development, 3, 43-67, 2010.
- 714 EPA: EPA National Air Pollutant Emission Trends Update, 1970–1997., Office of Air  
715 Quality Planning and Standards, Research Triangle Park, NC, USA, 1998.
- 716 EPA, U.: Guidance on the use of models and other analyses for demonstrating attainment  
717 of air quality goals for ozone, PM<sub>2.5</sub>, and regional haze, EPA-454/B07-002, 2007.
- 718 EPA, U.: Air Quality Modeling Final Rule Technical Support Document, EPA Office of  
719 Air Quality Planning and Standards 2011.
- 720 Fountoukis, C., and Nenes, A.: ISORROPIA II: a computationally efficient  
721 thermodynamic equilibrium model for  $K^+$ – $Ca^{2+}$ – $Mg^{2+}$ – $NH_4^+$ – $Na^+$ – $SO_4^{2-}$ – $NO_3^-$ –  
722  $Cl^-$ – $H_2O$  aerosols, Atmospheric Chemistry and Physics, 7, 4639-4659, 2007.
- 723 Fowler, D., Pitcairn, C. E. R., Sutton, M. A., Flechard, C., Loubet, B., Coyle, M., and  
724 Munro, R. C.: The mass budget of atmospheric ammonia in woodland within 1 km  
725 of livestock buildings, Environmental Pollution, 102, 343-348,  
726 [http://dx.doi.org/10.1016/S0269-7491\(98\)80053-5](http://dx.doi.org/10.1016/S0269-7491(98)80053-5), 1998.
- 727 Gilbert, R. O.: Statistical methods for environmental pollution monitoring, John Wiley &  
728 Sons, 1987.



- 729 Hand, J., Schichtel, B., Malm, W., and Pitchford, M.: Particulate sulfate ion concentration  
730 and SO<sub>2</sub> emission trends in the United States from the early 1990s through 2010,  
731 Atmospheric Chemistry and Physics, 12, 10353-10365, 2012.
- 732 Heald, C. L., Collett Jr, J., Lee, T., Benedict, K., Schwandner, F., Li, Y., Clarisse, L.,  
733 Hurtmans, D., Van Damme, M., and Clerbaux, C.: Atmospheric ammonia and  
734 particulate inorganic nitrogen over the United States, Atmospheric Chemistry and  
735 Physics, 12, 10295-10312, 2012.
- 736 Hertel, O., Skjøth, C. A., Løfstrøm, P., Geels, C., Frohn, L. M., Ellermann, T., and Madsen,  
737 P. V.: Modelling Nitrogen Deposition on a Local Scale—A Review of the Current  
738 State of the Art, Environmental Chemistry, 3, 317-337,  
739 <http://dx.doi.org/10.1071/EN06038>, 2006.
- 740 Horii, C. V., William Munger, J., Wofsy, S. C., Zahniser, M., Nelson, D., and Barry  
741 McManus, J.: Atmospheric reactive nitrogen concentration and flux budgets at a  
742 Northeastern U.S. forest site, Agricultural and Forest Meteorology, 136, 159-174,  
743 <http://dx.doi.org/10.1016/j.agrformet.2006.03.005>, 2006.
- 744 Houyoux, M., Vukovich, J., Brandmeyer, J., Seppanen, C., and Holland, A.: Sparse Matrix  
745 Operator Kernel Emissions Modeling System-SMOKE User Manual, Prepared by  
746 MCNC-North Carolina Supercomputing Center, Environmental Programs,  
747 Research Triangle Park, NC, 2000.
- 748 Ianniello, A., Spataro, F., Esposito, G., Allegrini, I., Rantica, E., Ancora, M., Hu, M., and  
749 Zhu, T.: Occurrence of gas phase ammonia in the area of Beijing (China),  
750 Atmospheric Chemistry and Physics, 10, 9487-9503, 2010.



- 751 Ianniello, A., Spataro, F., Esposito, G., Allegrini, I., Hu, M., and Zhu, T.: Chemical  
752 characteristics of inorganic ammonium salts in PM<sub>2.5</sub> in the atmosphere of Beijing  
753 (China), *Atmospheric Chemistry and Physics*, 11, 10803-10822, 10.5194/acp-11-  
754 10803-2011, 2011.
- 755 Langridge, J. M., Lack, D., Brock, C. A., Bahreini, R., Middlebrook, A. M., Neuman, J.  
756 A., Nowak, J. B., Perring, A. E., Schwarz, J. P., Spackman, J. R., Holloway, J. S.,  
757 Pollack, I. B., Ryerson, T. B., Roberts, J. M., Warneke, C., de Gouw, J. A., Trainer,  
758 M. K., and Murphy, D. M.: Evolution of aerosol properties impacting visibility and  
759 direct climate forcing in an ammonia-rich urban environment, *Journal of*  
760 *Geophysical Research: Atmospheres*, 117, D00V11, 10.1029/2011jd017116, 2012.
- 761 Lee, T., Yu, X.-Y., Kreidenweis, S. M., Malm, W. C., and Collett, J. L.: Semi-continuous  
762 measurement of PM<sub>2.5</sub> ionic composition at several rural locations in the United  
763 States, *Atmospheric Environment*, 42, 6655-6669,  
764 <http://dx.doi.org/10.1016/j.atmosenv.2008.04.023>, 2008.
- 765 Lelieveld, J., Evans, J. S., Fnais, M., Giannadaki, D., and Pozzer, A.: The contribution of  
766 outdoor air pollution sources to premature mortality on a global scale, *Nature*, 525,  
767 367-371, 10.1038/nature15371, 2015.
- 768 Li, Y., Schwandner, F. M., Sewell, H. J., Zivkovich, A., Tigges, M., Raja, S., Holcomb, S.,  
769 Molenaar, J. V., Sherman, L., Archuleta, C., Lee, T., and Collett Jr., J. L.:  
770 Observations of ammonia, nitric acid, and fine particles in a rural gas production  
771 region, *Atmospheric Environment*, 83, 80-89,  
772 <http://dx.doi.org/10.1016/j.atmosenv.2013.10.007>, 2014.



- 773 Lin, Y.-C., Cheng, M.-T., Ting, W.-Y., and Yeh, C.-R.: Characteristics of gaseous HNO<sub>2</sub>,  
774 HNO<sub>3</sub>, NH<sub>3</sub> and particulate ammonium nitrate in an urban city of Central Taiwan,  
775 Atmospheric Environment, 40, 4725-4733,  
776 <http://dx.doi.org/10.1016/j.atmosenv.2006.04.037>, 2006.
- 777 Marchetto, A., Rogora, M., and Arisci, S.: Trend analysis of atmospheric deposition data:  
778 A comparison of statistical approaches, Atmospheric Environment, 64, 95-102,  
779 <http://dx.doi.org/10.1016/j.atmosenv.2012.08.020>, 2013.
- 780 Massman, W. J.: A review of the molecular diffusivities of H<sub>2</sub>O, CO<sub>2</sub>, CH<sub>4</sub>, CO, O<sub>3</sub>, SO<sub>2</sub>,  
781 NH<sub>3</sub>, N<sub>2</sub>O, NO, and NO<sub>2</sub> in air, O<sub>2</sub> and N<sub>2</sub> near STP, Atmospheric Environment,  
782 32, 1111-1127, [http://dx.doi.org/10.1016/S1352-2310\(97\)00391-9](http://dx.doi.org/10.1016/S1352-2310(97)00391-9), 1998.
- 783 Meng, Z., Lin, W., Jiang, X., Yan, P., Wang, Y., Zhang, Y., Jia, X., and Yu, X.:  
784 Characteristics of atmospheric ammonia over Beijing, China, Atmospheric  
785 Chemistry and Physics, 11, 6139-6151, 2011.
- 786 Pan, Y., Wang, Y., Tang, G., and Wu, D.: Wet and dry deposition of atmospheric nitrogen  
787 at ten sites in Northern China, Atmospheric Chemistry and Physics, 12, 6515-6535,  
788 2012.
- 789 Park, R. J., Jacob, D. J., Kumar, N., and Yantosca, R. M.: Regional visibility statistics in  
790 the United States: Natural and transboundary pollution influences, and implications  
791 for the Regional Haze Rule, Atmospheric Environment, 40, 5405-5423,  
792 <http://dx.doi.org/10.1016/j.atmosenv.2006.04.059>, 2006.
- 793 Parry, M. L., Canziani, O. F., Palutikof, J. P., van der Linden, P. J., and Hanson, C. E.:  
794 IPCC, 2007: climate change 2007: impacts, adaptation and vulnerability.  
795 Contribution of working group II to the fourth assessment report of the



- 796 intergovernmental panel on climate change, in, Cambridge University Press,  
797 Cambridge, 2007.
- 798 Paulot, F., Jacob, D. J., and Henze, D. K.: Sources and processes contributing to nitrogen  
799 deposition: an adjoint model analysis applied to biodiversity hotspots worldwide,  
800 Environmental Science & Technology, 47, 3226-3233, 10.1021/es3027727, 2013.
- 801 Pinder, R. W., Walker, J. T., Bash, J. O., Cady-Pereira, K. E., Henze, D. K., Luo, M.,  
802 Osterman, G. B., and Shephard, M. W.: Quantifying spatial and seasonal variability  
803 in atmospheric ammonia with in situ and space-based observations, Geophysical  
804 Research Letters, 38, L04802, 10.1029/2010GL046146, 2011.
- 805 Plessow, K., Spindler, G., Zimmermann, F., and Matschullat, J.: Seasonal variations and  
806 interactions of N-containing gases and particles over a coniferous forest, Saxony,  
807 Germany, Atmospheric Environment, 39, 6995-7007,  
808 <http://dx.doi.org/10.1016/j.atmosenv.2005.07.046>, 2005.
- 809 Prenni, A., Chen, X., Hecobian, A., Kreidenweis, S., Collett, J., and Schichtel, B.:  
810 Measurements of gas phase reactive nitrogen during two wildfires in Colorado,  
811 AGU Fall Meeting Abstracts, 2012, 0618.
- 812 Prenni, A., Levin, E., Benedict, K., Sullivan, A., Schurman, M., Gebhart, K., Day, D.,  
813 Carrico, C., Malm, W., and Schichtel, B.: Gas-phase reactive nitrogen near Grand  
814 Teton National Park: Impacts of transport, anthropogenic emissions, and biomass  
815 burning, Atmospheric Environment, 89, 749-756, 2014.
- 816 Puchalski, M. A., Sather, M. E., Walker, J. T., Lehmann, C. M., Gay, D. A., Mathew, J.,  
817 and Robarge, W. P.: Passive ammonia monitoring in the United States: Comparing



- 818 three different sampling devices, *Journal of Environmental Monitoring*, 13, 3156-  
819 3167, 2011.
- 820 Pul, A., Hertel, O., Geels, C., Dore, A., Vieno, M., Jaarsveld, H., Bergström, R., Schaap,  
821 M., and Fagerli, H.: Modelling of the Atmospheric Transport and Deposition of  
822 Ammonia at a National and Regional Scale, in: *Atmospheric Ammonia*, edited by:  
823 Sutton, M., Reis, S., and Baker, S. H., Springer Netherlands, 301-358, 2009.
- 824 Reche, C., Viana, M., Pandolfi, M., Alastuey, A., Moreno, T., Amato, F., Ripoll, A., and  
825 Querol, X.: Urban NH<sub>3</sub> levels and sources in a Mediterranean environment,  
826 *Atmospheric Environment*, 57, 153-164, 10.1016/j.atmosenv.2012.04.021, 2012.
- 827 Schwartz, J., and Neas, L. M.: Fine Particles Are More Strongly Associated than Coarse  
828 Particles with Acute Respiratory Health Effects in Schoolchildren, *Epidemiology*,  
829 11, 6-10, 2000.
- 830 Skamarock, W. C., Klemp, J. B., Dudhia, J., Gill, D. O., Barker, D. M., Wang, W., and  
831 Powers, J. G.: A description of the advanced research WRF version 2, DTIC  
832 Document, 2005.
- 833 Sutton, M. A., Dragosits, U., Tang, Y. S., and Fowler, D.: Ammonia emissions from non-  
834 agricultural sources in the UK, *Atmospheric Environment*, 34, 855-869,  
835 [http://dx.doi.org/10.1016/S1352-2310\(99\)00362-3](http://dx.doi.org/10.1016/S1352-2310(99)00362-3), 2000.
- 836 Sutton, M. A., Erisman, J. W., Dentener, F., and Möller, D.: Ammonia in the environment:  
837 from ancient times to the present, *Environmental Pollution*, 156, 583-604, 2008.
- 838 Sutton, M. A., Reis, S., Riddick, S. N., Dragosits, U., Nemitz, E., Theobald, M. R., Tang,  
839 Y. S., Braban, C. F., Vieno, M., and Dore, A. J.: Towards a climate-dependent



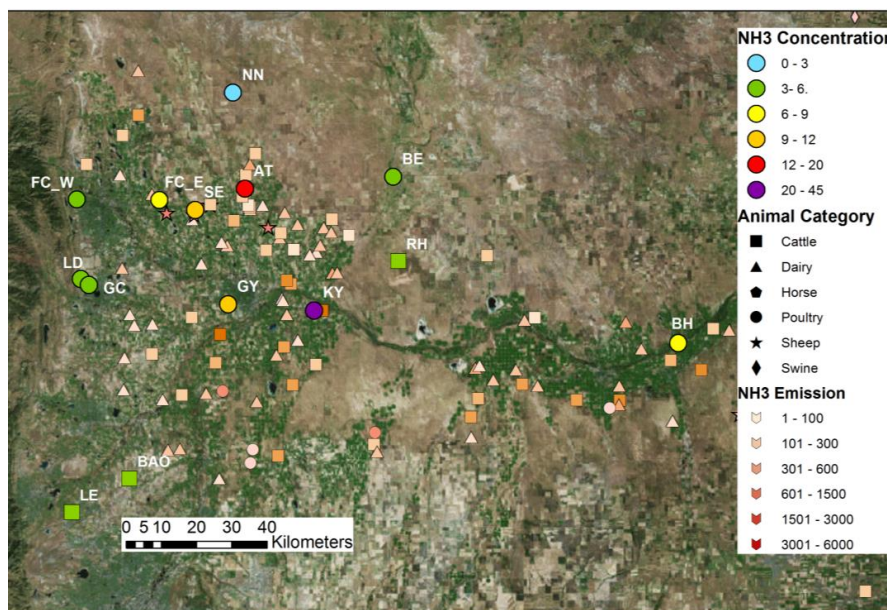
- 840 paradigm of ammonia emission and deposition, Philosophical Transactions of the  
841 Royal Society of London B: Biological Sciences, 368, 20130166, 2013.
- 842 Theil, H.: A Rank-Invariant Method of Linear and Polynomial Regression Analysis, in:  
843 Henri Theil's Contributions to Economics and Econometrics, edited by: Raj, B.,  
844 and Koerts, J., Advanced Studies in Theoretical and Applied Econometrics,  
845 Springer Netherlands, 345-381, 1992.
- 846 Todd, R. W., Cole, N. A., Waldrip, H. M., and Aiken, R. M.: Arrhenius equation for  
847 modeling feedyard ammonia emissions using temperature and diet crude protein,  
848 Journal of Environmental Quality, 42, 666-671, 2013.
- 849 USEPA: National Emission Inventory – Ammonia Emissions from Animal Husbandry –  
850 Draft Report, US Environmental Protection Agency, Washington, D.C., Jan. 30,  
851 2004, 2004.
- 852 Van Damme, M., Wichink Kruit, R., Schaap, M., Clarisse, L., Clerbaux, C., Coheur, P. F.,  
853 Dammers, E., Dolman, A., and Erisman, J.: Evaluating 4 years of atmospheric  
854 ammonia (NH<sub>3</sub>) over Europe using IASI satellite observations and LOTOS -  
855 EUROS model results, Journal of Geophysical Research: Atmospheres, 119, 9549-  
856 9566, 2014.
- 857 Van Damme, M., Clarisse, L., Dammers, E., Liu, X., Nowak, J. B., Clerbaux, C., Flechard,  
858 C. R., Galy-Lacaux, C., Xu, W., Neuman, J. A., Tang, Y. S., Sutton, M. A., Erisman,  
859 J. W., and Coheur, P. F.: Towards validation of ammonia (NH<sub>3</sub>) measurements  
860 from the IASI satellite, Atmospheric Measurement Techniques, 8, 1575-1591,  
861 10.5194/amt-8-1575-2015, 2015.



- 862 Walker, J. T., Whittall, D. R., Robarge, W., and Paerl, H. W.: Ambient ammonia and  
863 ammonium aerosol across a region of variable ammonia emission density,  
864 Atmospheric Environment, 38, 1235-1246,  
865 <http://dx.doi.org/10.1016/j.atmosenv.2003.11.027>, 2004.
- 866 Whitburn, S., Van Damme, M., Kaiser, J. W., Van Der Werf, G. R., Turquety, S., Hurtmans,  
867 D., Clarisse, L., Clerbaux, C., and Coheur, P.-F.: Ammonia emissions in tropical  
868 biomass burning regions: Comparison between satellite-derived emissions and  
869 bottom-up fire inventories, Atmospheric Environment, 121, 42-54, 2015.
- 870 Whitburn, S., Van Damme, M., Clarisse, L., Bauduin, S., Heald, C., Hadji - Lazaro, J.,  
871 Hurtmans, D., Zondlo, M., Clerbaux, C., and Coheur, P. F.: A flexible and robust  
872 neural network IASI - NH<sub>3</sub> retrieval algorithm, Journal of Geophysical Research:  
873 Atmospheres, 2016.
- 874 Zbieranowski, A. L., and Aherne, J.: Spatial and temporal concentration of ambient  
875 atmospheric ammonia in southern Ontario, Canada, Atmospheric Environment, 62,  
876 441-450, 10.1016/j.atmosenv.2012.08.041, 2012.
- 877 Zhu, L., Henze, D., Cady - Pereira, K., Shephard, M., Luo, M., Pinder, R., Bash, J., and  
878 Jeong, G. R.: Constraining US ammonia emissions using TES remote sensing  
879 observations and the GEOS - Chem adjoint model, Journal of Geophysical  
880 Research: Atmospheres, 118, 3355-3368, 2013.
- 881
- 882

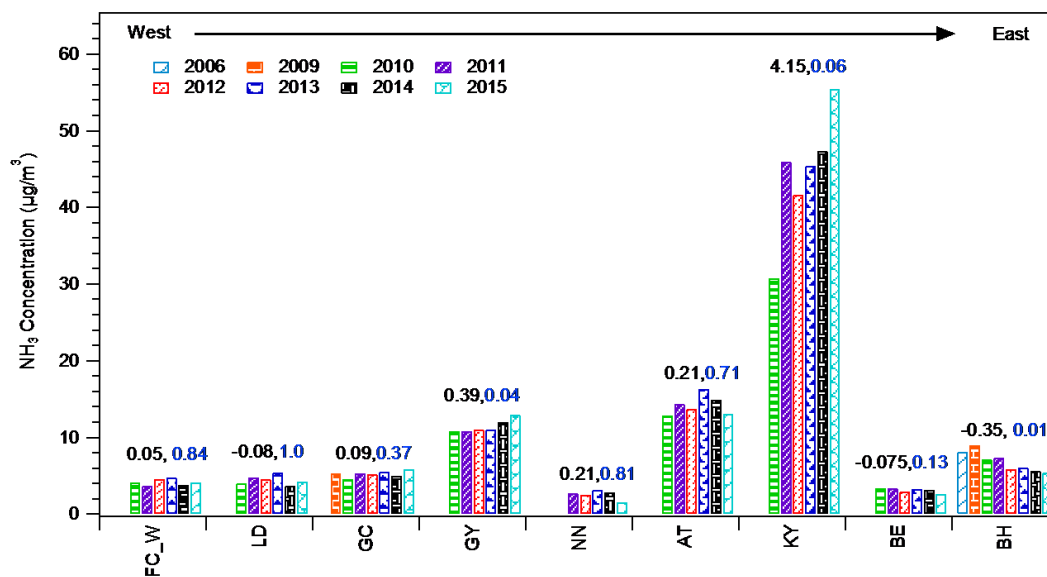


883 **Figure**



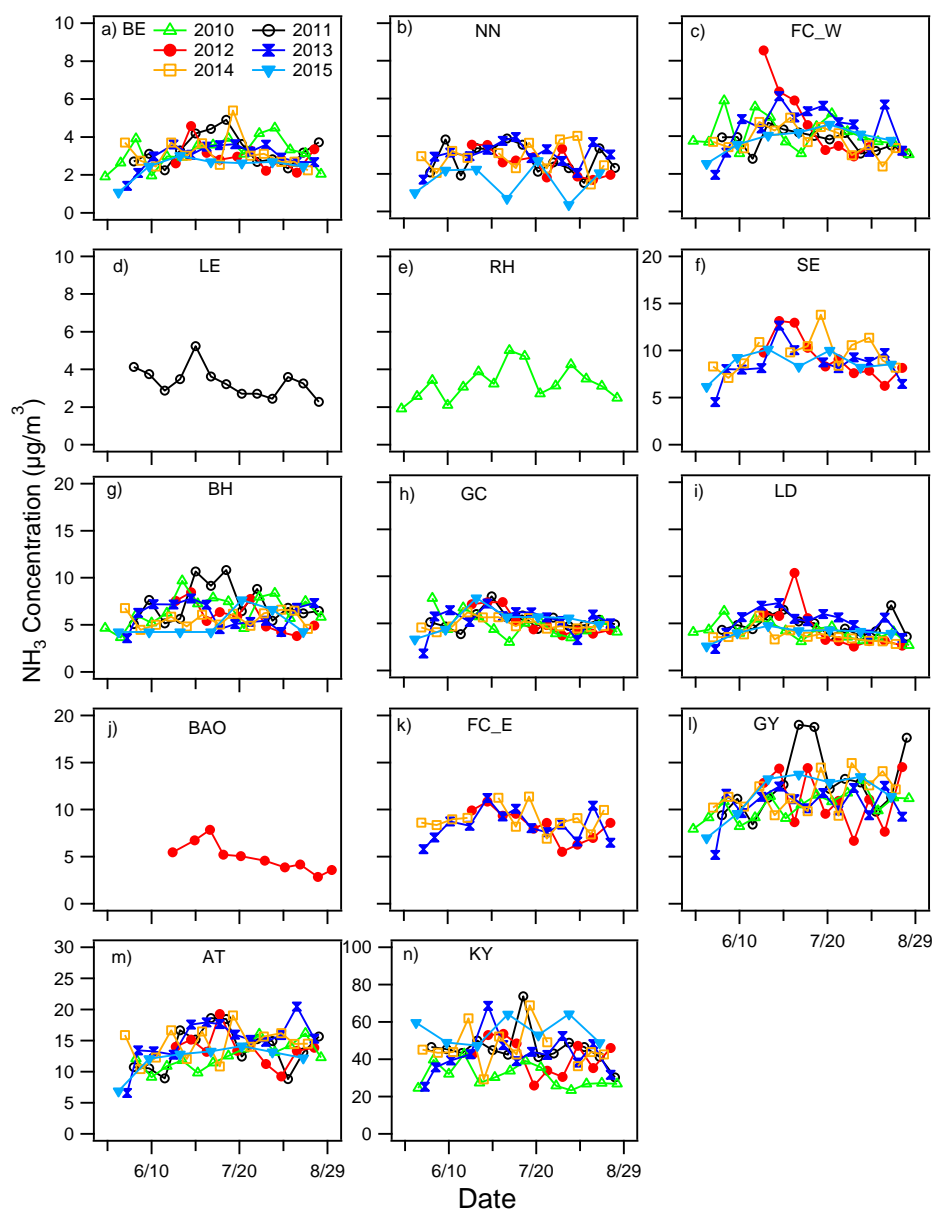
884

885 Fig.1.  $\text{NH}_3$  concentrations (unit:  $\mu\text{g}/\text{m}^3$ ) and feedlot emissions (unit: tons/year) in northeast  
886 Colorado. All sites indicated by circles include at least 3 years measurement in summer.  
887  $\text{NH}_3$  concentrations at the RH, LE and BAO sites (squares) were only measured in the  
888 summers of 2010, 2011 and 2012, respectively. The predicted annual  $\text{NH}_3$  emissions are  
889 calculated based on Eq. 4.

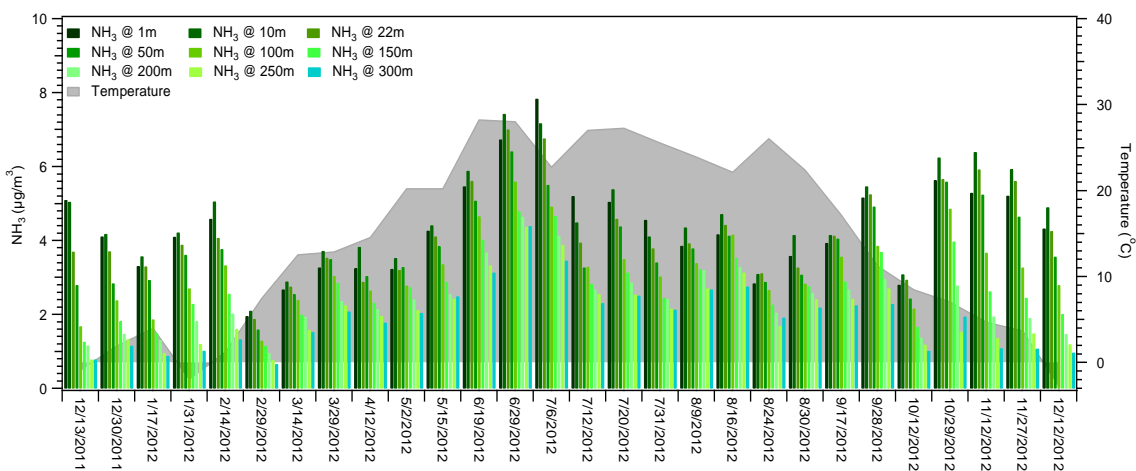


890

891 Fig.2. Average concentrations of  $\text{NH}_3$  in each summer (approximately June through August)  
 892 across the nine sites. In 2006 (07/06-08/10), ambient  $\text{NH}_3$  concentrations were sampled by  
 893 a URG denuder (daily) at the BH site; in 2009 (06/11-08/27) ambient  $\text{NH}_3$  concentrations  
 894 were sampled by a URG denuder (weekly) at the GC and BH sites; in 2010 (06/17-09/02),  
 895 2011 (06/16-08/31), 2012 (06/21-08/29), 2013 (06/20-08/29), 2014(06/19-08/28) and  
 896 2015(06/23-09/01), ambient  $\text{NH}_3$  concentrations were all sampled by Radiello ammonia  
 897 passive samplers across all the sites. The slope of the Theil regression and “p-value” for  
 898 each site are labeled in black and blue, respectively



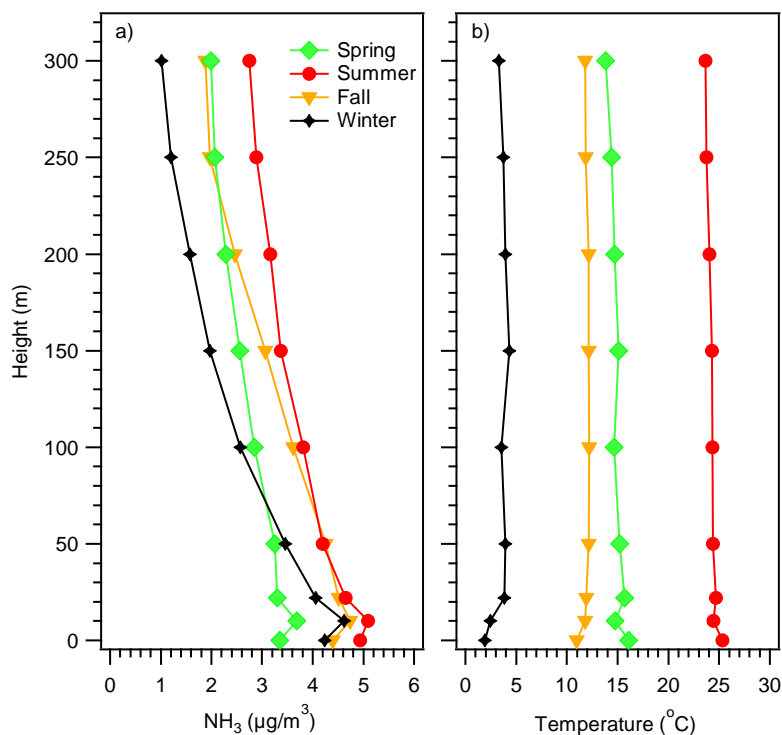
899 Fig.3. Temporal variations of  $\text{NH}_3$  concentrations (unit:  $\mu\text{g}/\text{m}^3$ ) at each site from 2010  
900 through 2015. Note the differences in the y-axis values.



901

902 Fig.4. Time series of vertical distribution of  $\text{NH}_3$  concentrations and surface temperature

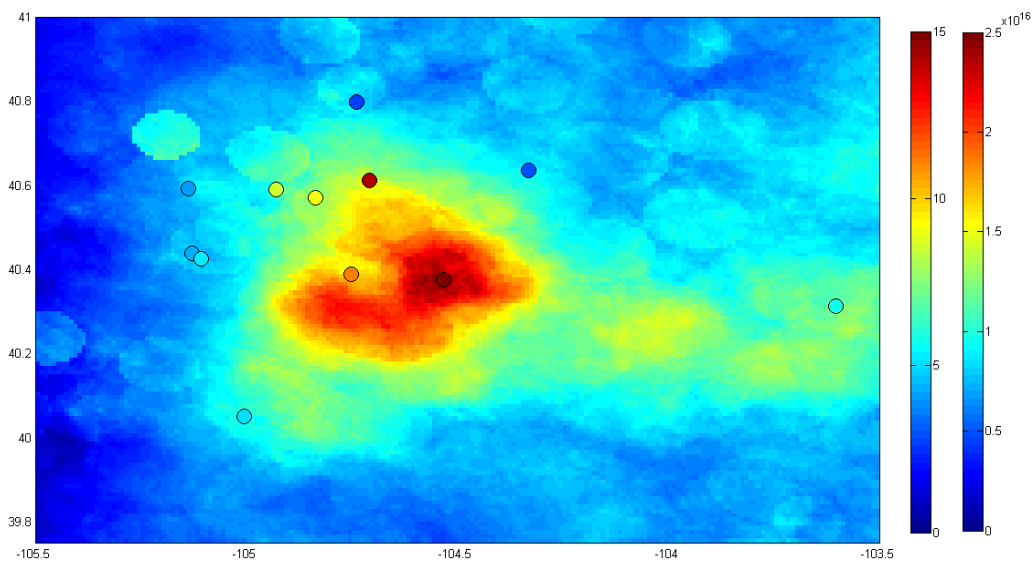
903 measured at the BAO tower from 12/13/2011 to 01/09/2013.



904

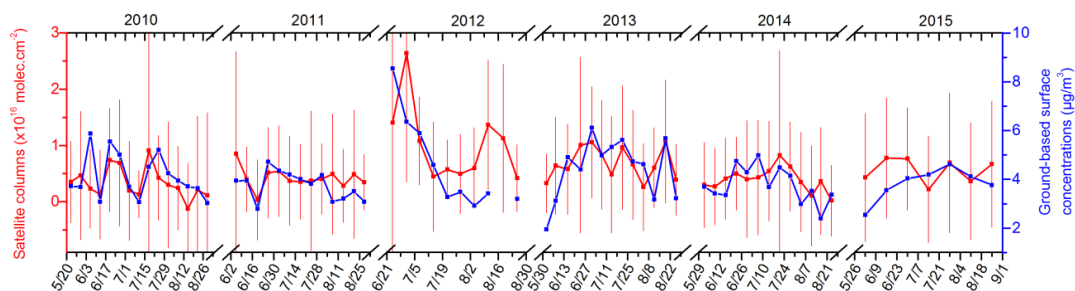
905 Fig.5. Comparison of seasonal average vertical profiles of (a)  $\text{NH}_3$  and (b) temperature

906 measured at the BAO tower from 12/13/2011 to 01/09/2013.



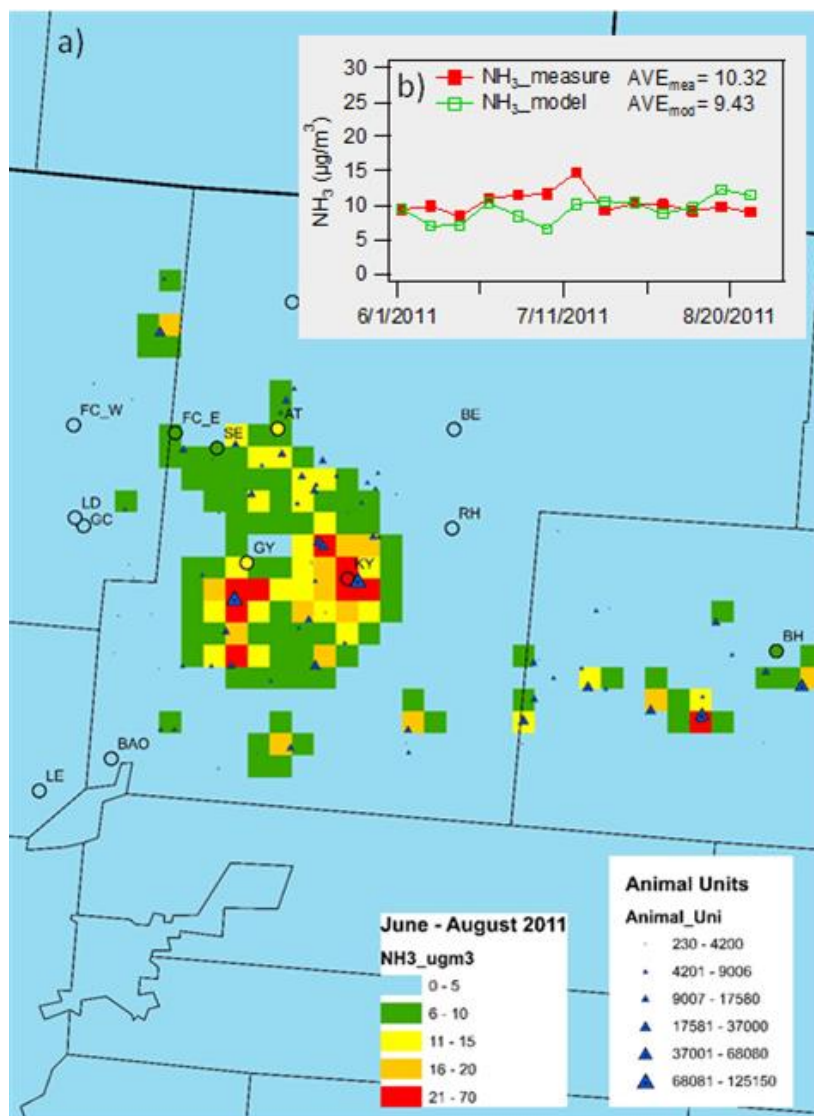
907

908 Fig.6. Radiello passive sampler surface  $\text{NH}_3$  concentrations ( $\mu\text{g}/\text{m}^3$ , left color bar) plotted  
909 on top of IASI- $\text{NH}_3$  satellite column retrievals ( $\text{molec}/\text{cm}^2$ , right color bar), both  
910 averaged for the summers of four years (2012- 2015). The BAO site was only sampled *in*  
911 *situ* in the summer of 2012.



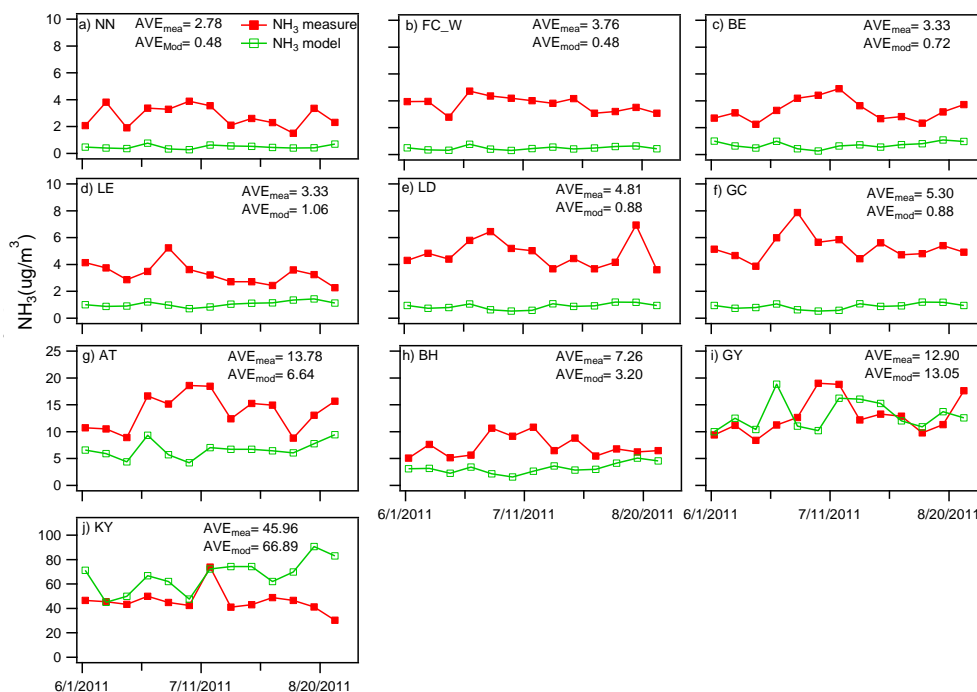
912

913 Fig.7. Time series of (bi-)weekly averaged IASI- $\text{NH}_3$  satellite column (red) and surface  
914 concentrations measured by Radiello passive sampler (blue) at FC\_W site. The error bars  
915 represent the standard deviation of the mean satellite column retrievals.



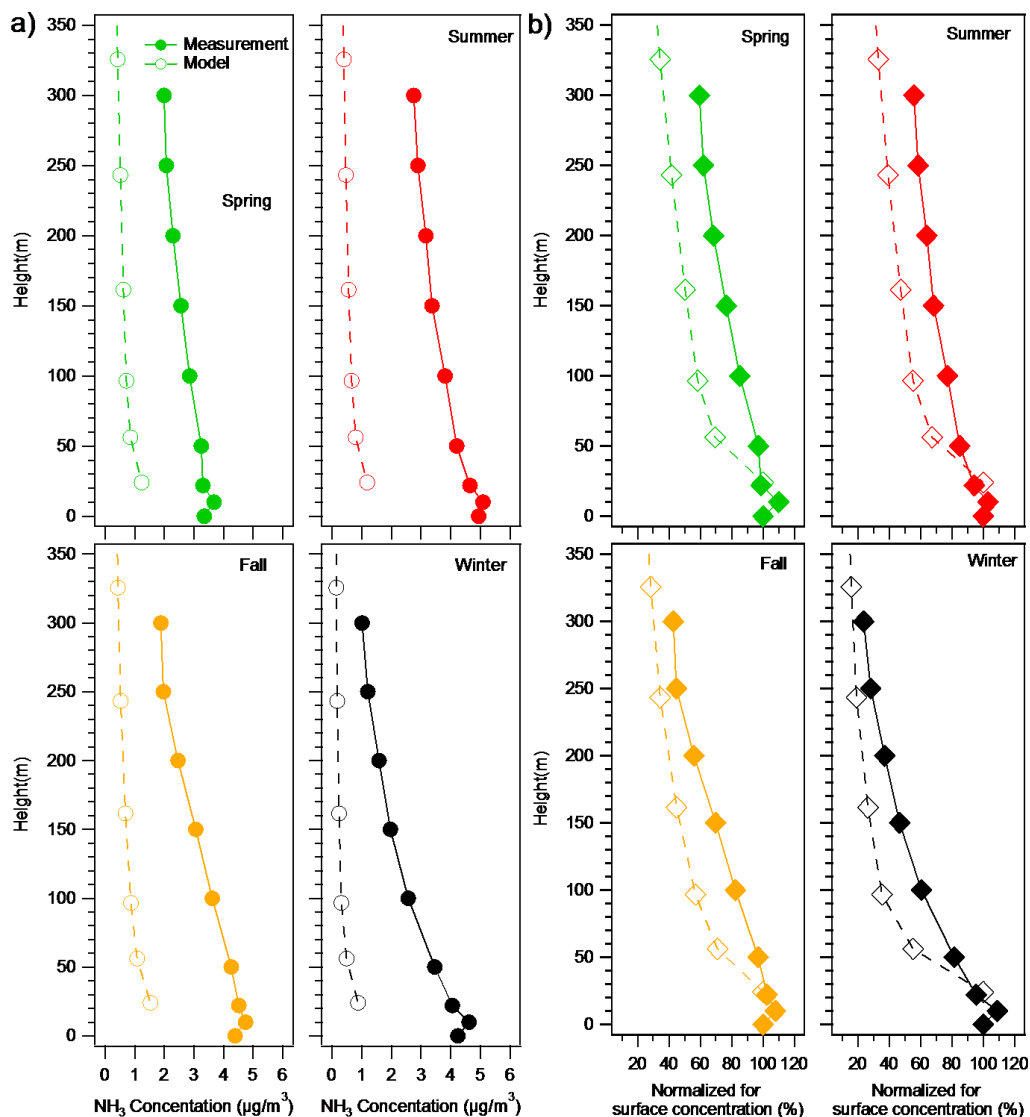
916

917 Fig.8. (a) Comparison of spatial patterns (circles correspond to concentrations measured  
918 and are superimposed on the modeled distribution) and (b) time series of average NH<sub>3</sub>  
919 concentrations measured by passive samplers and modeled by CAMx in the summer of  
920 2011 (06/02/2011-08/31/2011). The time series in panel (b) represent the average NH<sub>3</sub>  
921 concentrations modeled (green) and measured (red) across the surface monitoring network.



922

923 Fig.9. Time series of weekly NH<sub>3</sub> concentrations measured (red) and modeled (green) in  
924 the summer of 2011(06/02/2011-08/31/2011) at all the sites each measurement site.



925 Fig.10 (a) Comparison of seasonal 2012 NH<sub>3</sub> concentrations ( $\mu\text{g}/\text{m}^3$ ) passive  
 926 measurements (solid lines) and 2011 CAMx modeling results (dashed lines); (b)  
 927 comparison of seasonal NH<sub>3</sub> passive measurements normalized by surface concentrations  
 928 (solid lines) and CAMx modeling results (dashed lines). Each profile is normalized such  
 929 that the concentration at the lowest level is set to 100.

930

931 **Table**

932

Table 1. Information on sampling sties

ID	Site Name	Type	Latitude	Longitude	Elevation(m)	Year*	Sampler type
LE	Louisville	Suburban	39.987	-105.151	1698	11	Passive
FC_W	Fort Collins_West	Suburban	40.589	-105.148	1570	10,11, 12, 13,14,15	Passive/UR G
LD	Loveland	Suburban	40.438	-105.127	1582	10,11, 12, 13,14,15	Passive
BAO	BAO Tower	Suburban	40.050	-105.004	1584	12**	Passive/UR G
GC	Golf Course	Golf course	40.426	-105.107	1551	10,11, 12, 13,14,15	Passive
FC_E	Fort Collins_East	Suburban – agricultural	40.591	-104.928	1562	12, 13,14	Passive
SE	Severance	Suburban – agricultural	40.572	-104.836	1550	12, 13,14,15	Passive
GY	Greeley	Suburban – agricultural	40.389	-104.751	1492	10,11, 12, 13,14,15	Passive
NN	Nunn	Rural	40.821	-104.701	1644	11,12, 13,14,15	Passive
BE	Briggsdale	Rural	40.635	-104.330	1481	10,11, 12, 13,14,15	Passive
RH	Ranch	Rural	40.473	-104.317	1475	10	Passive
AT	Ault	Rural- agricultural	40.612	-104.709	1514	11,12, 13,14,15	Passive
KY	Kersey	Rural- agricultural	40.377	-104.532	1403	10,11, 12, 13,14,15	Passive
BH	Brush	Rural- agricultural	40.313	-103.602	1286	10,11, 12, 13,14,15	Passive/UR G

933 \* Sampling period: 05/20/2010-09/02/2010; 06/02/2011-08/31/2011; 06/21/2012-08/29/2012; 05/30/2013-

934 08/29/2013; 05/29/2014-08/28/2014; 05/26/2015-09/01/2015

935 \*\* Even though a one year measurement were conduct at BAO site from 12/13/2011 to 01/09/2013, the

936 summer (06/19/2012-08/30/2012) average of NH<sub>3</sub> concentration were reported in Figure 1 to compare the937 NH<sub>3</sub> concentrations at other sites.

938



Table 2. Summary of summer  $\text{NH}_3$  concentrations (units:  $\mu\text{g}/\text{m}^3$ ) measured from 2010 to 2015

Site	All years			2010			2011			2012			2013			2014			2015			
	Ave	Max	Min	Ave	Max	Min	Ave	Max	Min	Ave	Max	Min	Ave	Max	Min	Ave	Max	Min	Ave	Max	Min	
LE	3.33	5.23	2.27	--	--	2.27	3.33	5.23	2.27	--	--	--	--	--	--	--	--	--	--	--	--	
FC_W	4.09	8.55	1.95	4.13	5.88	3.02	3.76	4.72	2.79	4.63	8.55	2.92	4.45	6.13	1.95	3.78	4.98	2.39	3.83	4.62	2.54	
LD	4.40	10.37	2.29	4.17	6.29	2.67	4.81	6.94	3.61	4.57	10.37	2.55	5.08	7.16	2.29	3.68	5.82	2.83	3.99	4.74	2.60	
BAO	5.09	7.84	2.85	--	--	--	--	--	--	5.09	7.84	2.85	--	--	--	--	--	--	--	--	--	--
GC	5.14	7.87	1.81	4.85	7.68	3.01	5.30	7.87	3.87	5.22	7.27	3.74	5.34	7.11	1.81	4.92	6.18	4.07	5.31	7.69	3.33	
FC_E	8.56	11.38	5.52	--	--	--	--	--	--	8.36	10.84	5.52	8.30	11.25	5.80	8.99	11.38	6.92	--	--	--	--
SE	9.10	13.79	4.52	--	--	--	--	--	--	9.34	13.14	6.24	8.52	12.67	4.52	9.70	13.79	7.10	8.66	10.13	6.18	
GY	11.34	19.02	5.19	10.39	13.11	7.94	12.90	19.02	8.40	11.07	14.51	6.68	10.52	12.54	5.19	11.72	14.95	9.35	11.63	13.75	7.00	
NN	2.66	4.01	0.35	--	--	--	2.78	3.88	1.51	2.59	3.54	1.68	3.01	3.95	1.69	2.84	4.01	1.43	1.60	2.70	0.35	
BE	3.07	5.40	1.09	3.18	4.48	1.90	3.33	4.90	2.55	2.99	4.58	2.12	3.00	3.62	1.42	3.15	5.40	2.24	2.43	3.02	1.09	
RH	3.27	5.01	1.90	3.27	5.01	1.90	--	--	--	--	--	--	--	--	--	--	--	--	--	--	--	--
AT	13.75	20.47	6.56	12.55	16.16	9.13	13.78	18.61	8.82	13.70	19.27	9.25	15.13	20.47	6.56	14.49	19.03	10.44	12.08	14.11	6.89	
KY	42.73	73.78	23.30	31.05	42.82	23.30	45.96	73.78	30.32	41.65	53.55	25.93	42.67	68.61	25.20	46.57	68.82	29.22	55.14	64.21	47.31	
BH	6.17	10.83	3.59	6.54	9.67	3.67	7.26	10.83	5.09	5.45	8.52	3.80	5.99	7.80	3.59	5.62	6.79	4.47	5.07	7.66	4.24	